

Slow-light frequency combs and dissipative Kerr solitons in coupled-cavity waveguides

J. P. Vasco and V. Savona

Institute of Theoretical Physics, Ecole Polytechnique Fédérale de Lausanne EPFL, CH-1015 Lausanne, Switzerland

We study Kerr frequency combs and dissipative Kerr solitons in silicon photonic crystal coupled-cavity waveguides (CCW) with globally optimized dispersion at telecom wavelengths. The corresponding threshold for comb generation is found to explicitly depend on the main CCW figures of merit, namely, mode volume, normal mode quality factor and slow-light group index. Our analysis is carried out by solving the non-linear dynamics of the CCW Bloch modes in presence of Kerr non-linearity and two-photon absorption. Our results open the way to CCW comb generation via dispersion engineering and slow-light enhancement.

I. INTRODUCTION

Kerr frequency combs have revolutionized several fields in optical sciences since they were first proposed in monolithic microresonators [1]. To date, they have been successfully applied to a vast variety of state-of-the-art technologies and highly sophisticated measurement techniques as ultra-high resolution spectroscopy [2, 3], massively parallel coherent optical communications [4], light detection and ranging (LIDAR) [5], optical-frequency synthesizers [6] and microphotonic astrocombs [7, 8]. Frequency combs in optical microresonators are generated by the interaction of either, a continuous-wave (cw) pump laser or pumped optical pulses [9], with the resonator modes via parametric four-wave mixing (FWM), assisted by the Kerr non-linearity of the material. This parametric process fulfills the energy conservation and is enhanced when the side bands created by FWM coincide with the resonator frequencies. Since the intensity-dependent refractive index induces a frequency shift on the modes, an increasing free spectral range (FSR) with frequency (anomalous dispersion) is required to compensate this effect and effectively produce equidistant spectral lines suitable to support the cascaded FWM [10]. When a high number of mode-locked modes are involved in this non-linear interaction and dissipation cannot be neglected, the complex non-linear dynamics may give rise to dissipative Kerr solitons (DKS), which arise as a double balance between non-linearity and dispersion (preserving their shape), as well as dissipation and parametric gain (preserving their amplitude) [11]. Moreover, multiple-soliton formations have become very interesting in the context of localized-state interactions [12–14], breather solitons [15–17] and soliton crystals [18, 19]. DKS are notably relevant because their corresponding spectra exhibit highly coherent frequency combs with perfect single-FSR spacing between side bands [20, 21], and dispersive waves in presence of high-order dispersion [22–25]. The latter is particularly important because it allows a further spanning of the frequency combs, highlighting the important role of dispersion engineering on parametric gain, and consequently, on comb generation [26]. Such task has been successfully achieved in non-linear microresonators by varying the ring geometrical parameters in order to tailor the dispersion for specific

comb functionalities [27–29]. Nevertheless, this geometry has a limited parameter space, thus restricting the choice of materials, operation wavelength and size of the final device. Recently, Fabry-Perot resonators have been proposed as appealing candidates for frequency comb generation since different methods to reshape the cavity dispersion can be applied [30, 31], however, advanced dispersion engineering still remains challenging.

In this work, we propose a coupled-cavity waveguide (CCW, also known as coupled-resonator optical waveguide or CROW) as a new candidate to efficiently generate low-threshold Kerr frequency combs and DKS. Similar to ring resonators, CCWs define a discrete spectrum of propagating modes which may trigger cascaded parametric FWM in the anomalous dispersion regime, and lead to a highly coherent comb if the waveguide dispersion is conveniently optimized. In fact, since their appearance two decades ago [32], CCWs have shown to be extremely flexible for advanced dispersion engineering and enhancement of non-linear phenomena via slow-light [33–38]. We show in Fig. 1(a) a schematic representation of the CCW studied in this work. The periodic waveguide is formed by a staggered distribution of cavities where first (dashed red) and second (dashed green) neighbor cavity-cavity coupling is assumed. The system is pumped with a cw source and a DKS is propagating along the waveguide direction y .

II. NON-LINEAR PHOTONIC CRYSTAL CCW

The system of Fig. 1(a) is realized with the waveguide of coupled L3 photonic crystal slab cavities shown in Fig. 1(b), where we have plotted the intensity profile of the displacement field $[\mathbf{D}(\mathbf{r}) = \epsilon(\mathbf{r})\vec{\mathcal{E}}(\mathbf{r})]$ at the boundary of the Brillouin zone. The photonic crystal is formed by a hexagonal lattice of holes, pitch $a = 400$ nm and hole radii $r = 0.25a$, etched in a silicon membrane of thickness $d = 0.55a$, and the L3 cavity is introduced by removing three holes along the ΓK direction of the lattice. This CCW configuration allows us to tune first and second neighbor coupling between the L3 cavities by varying the size of the red and green holes, respectively, and optimize the out-of-plane losses by varying the position and size of the white ones. The waveguide of Fig. 1(b) has been

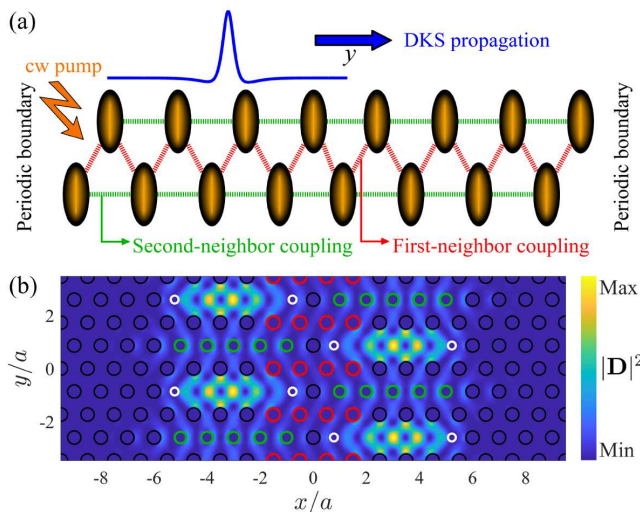


FIG. 1. (a) Schematic representation of a CCW system with first and second neighbor cavity coupling. The system is pumped with a cw source and a DKS propagates along the waveguide direction y . (b) Photonic crystal CCW formed by coupled L3 cavities where the red and green holes are allowed to vary in size to tune the first and second neighbor coupling, respectively, while the out-of-plane losses of the waveguide Bloch modes is optimized by varying the position and size of the white holes. The intensity profile of the displacement field $[\mathbf{D}(\mathbf{r}) = \epsilon(\mathbf{r})\vec{\mathcal{E}}(\mathbf{r})]$ is shown at the boundary of the Brillouin zone.

previously proposed as a compact CCW with outstanding figures of merit obtained via automated global optimization [38] and successfully measured experimentally [39, 40]. Here, we adopt the design with largest averaged group index and small second order dispersion reported in Ref. 38 with parameters $(\Delta r_1, \Delta r_2, \Delta r_3, \Delta x) = (-0.0049, -0.0340, -0.1016, 0.2204)a$, where $r_1 = r + \Delta r_1$, $r_2 = r + \Delta r_2$ and $r_3 = r + \Delta r_3$ are the radii of the red, green and white holes, respectively, and Δx is the outward displacement of the latter ones. The dispersion relation ν_α of the waveguide and decay rates γ_α of the Bloch modes of momentum α are calculated with the guided mode expansion method (GME) [41] for a system length of $M = 400$ cavities (400 normal modes within the Brillouin zone of the CCW) with period $l = \sqrt{3}a$ (waveguide length $L = Ml$), while the non-linear mode volume is computed with a commercial FDTD solver [42] and found to be $V_c = 0.345 \mu\text{m}^3$. This sample length represents a good compromise between total number of normal modes [avoiding finite-size effects in the coupled mode equations Eq. (C39)] and robustness to fabrication disorder [40, 43]. Silicon parameters at telecom frequencies are considered for the material, namely, dielectric constant $\epsilon = 12.04$, Kerr coefficient $n_2 = 5.52 \times 10^{-18} \text{ m}^2/\text{W}$ and two-photon absorption (TPA) coefficient $\beta_{\text{TPA}} = 1 \times 10^{-11} \text{ m/W}$ [44]. The GME dispersion relation, second order dispersion and group index are shown in Fig. 2(a)-2(c), respectively, for which

red and blue segments correspondingly highlight the regions of normal and anomalous dispersion. Notice that these dispersion curves are valid for a straight waveguide with periodic boundary conditions, nevertheless, we expect them to describe very well a close loop of coupled cavities as bending losses is usually very small, with respect to out-of-plane losses, in photonic crystal geometries [45]. The system is pumped at $a\alpha_0 = 1.2742$, where $\nu_{\alpha_0} = 193.39 \text{ THz}$, $(ac)^{-1}(d^2\nu/\alpha^2)_{\alpha_0} = 8.63 \times 10^{-4}$, $n_{g,\alpha_0} = 119.34$ and the normal mode quality factor is $Q_{\alpha_0} = 5.72 \times 10^4$. This sets an internal mode threshold given by

$$|\mathcal{A}_{\alpha_0}|_{\text{th}}^2 = \frac{\epsilon V_c}{2ln_{g,\alpha_0}n_2Q_{\alpha_0}}f(\kappa) = 138 \text{ mW}, \quad (1)$$

where \mathcal{A}_{α_0} is the slowly-varying amplitude of the Bloch mode α_0 , and $f(\kappa) = (\sqrt{1 + \kappa^2} + 2\kappa)/(1 - 3\kappa^2)$, with $\kappa = c\beta_{\text{TPA}}/(2n_2\omega_{\alpha_0})$, is a function of the material parameters only which gives $f(\kappa = 0.2236) = 1.73$ for silicon at $\omega_{\alpha_0}/2\pi = \nu_{\alpha_0} = 193.39 \text{ THz}$, and reduces to $f(\kappa = 0) = 1$ for $\beta_{\text{TPA}} = 0$. This result is particularly remarkable because, even by considering that TPA increases the threshold by a factor of 1.73, $|\mathcal{A}_{\alpha_0}|_{\text{th}}^2 = 138 \text{ mW}$ is still one order of magnitude smaller than in typical mm-size crystalline non-linear ring resonators [46]. Equation (1) undoubtedly strengthens the potential capabilities of CCW structures for low-threshold comb generation. While the factor V/Q also enters in the expression for the internal mode threshold of ring resonators [47–49], CCWs can drastically decrease this minimal power in the slow-light regime, i.e., for $n_{g,\alpha_0} \gg \sqrt{\epsilon}$. Such structural effect allows to access the rich physics of DKS in CCWs at much lower powers than in their monolithic counterparts even in presence of strong TPA, which is the main source of non-linear losses in silicon structures at telecom wavelengths [50, 51]. It is worth emphasizing that, since we are not specifying any particular coupling architecture with the external pump, we are referring to the internal mode threshold which scales as $1/Q$, and not to the external power threshold which is found to scale as $1/Q^2$ for ring resonators at critical coupling with the external source [52]. While the latter is an important parameter to set the excitation power in an experimental setup, the former quantity, also called the minimum intracavity power for comb generation [46], gives the corresponding effective power into the specific normal mode of the system. We plot in Fig. 2(d) the driven intensity $|\mathcal{F}_{\alpha_0}|^2$, in $|\mathcal{A}_{\alpha_0}|_{\text{th}}^2$ units, evaluated at threshold (continuous red lines) and at the bistability boundaries (continuous blue curves), as a function of the laser detuning $\sigma_{\alpha_0} = \Omega_0 - \omega_{\alpha_0}$ in units of γ_{α_0} , where the dashed lines are the corresponding curves for $\beta_{\text{TPA}} = 0$. The effects of TPA on the threshold are clearly seen in this plot, moreover, the hysteresis region (where the system has bistable states) is red-shifted and the area between the bistability boundaries is significantly reduced. Hence, the system needs to be pumped stronger and the laser frequency has to be further decreased to see Kerr frequency combs and DKS

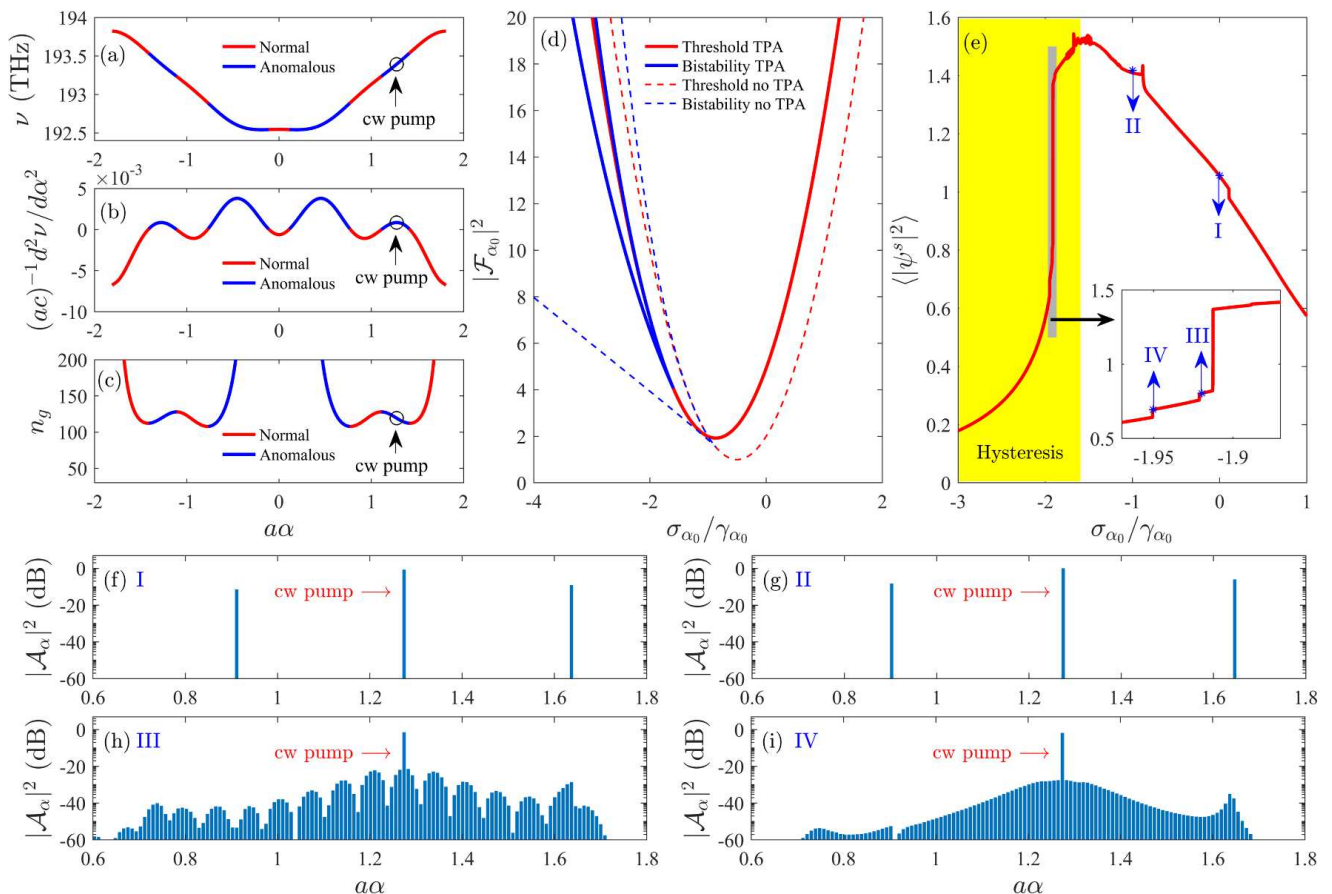


FIG. 2. (a) Dispersion relation, (b) second order dispersion, and (c) group index in the Brillouin zone of a photonic crystal CCW of 400 L3 cavities. Red and blue curves are where the dispersion is normal and anomalous, respectively. The waveguide is pumped at $a\alpha_0 = 1.2742$. (d) Threshold (red curve) and bistability boundaries (blue curves) determined by the external pump intensity $|\mathcal{F}_{\alpha_0}|^2$ as a function of the laser detuning σ_{α_0} . Dashed curves are for $\beta_{\text{TPA}} = 0$. (e) Averaged intra-waveguide power of the CCW in the steady state as a function of σ_{α_0} for $|\mathcal{F}_{\alpha_0}|^2 = 6|\mathcal{A}_{\alpha_0}|_{\text{th}}^2$. Hysteresis arises in the yellow region $\sigma_{\alpha_0} < -\gamma_{\alpha_0}\sqrt{3}\rho(\kappa)/2$ with $\rho(\kappa = 0.2236) = 1.84$, and the inset corresponds to a zoom of the rectangular gray area where the discrete steps, signature of switching between soliton states, appear. The corresponding frequency combs at the marked points I-IV in (e) are respectively shown in (f) supercritical Turing pattern of 40-FSR (355.2 GHz) repetition rate, (g) supercritical Turing pattern of 41-FSR (363.3 GHz) repetition rate, (h) soliton molecule of two pulses with single FSR (9.1 GHz) repetition rate, and (i) soliton pulse with single FSR repetition rate. All power quantities are given in dB units relatively to the threshold $|\mathcal{A}_{\alpha_0}|_{\text{th}}^2$, while detunings are in γ_{α_0} units.

in presence of TPA.

III. FREQUENCY COMB AND DKS SOLUTIONS

In order to find the possible steady state solutions determined by the non-linear CCW dynamics, we carry out a frequency scan at $|\mathcal{F}_{\alpha_0}|^2 = 6|\mathcal{A}_{\alpha_0}|_{\text{th}}^2$ in Fig. 2(d) within the $\sigma_{\alpha_0}/\gamma_{\alpha_0}$ interval $[-3, 1]$. The dynamical non-linear coupled-mode equations Eq. (C39) are thus propagated in time for each σ_{α_0} value along this trajectory using an explicit Runge-Kutta integrator and fast Fourier transform (see Ref. 53) until the steady state is reached. Our simulation takes into account the momentum-dependent decay rate γ_{α} of the Bloch modes,

and the initial condition of the integrator is a sharp Gaussian pulse $\psi(y, 0) = \exp[-0.5(y/l)^2]$, where $\psi(y, t) = \sum_{\alpha} \mathcal{A}_{\alpha}(t)e^{i\sigma_{\alpha}t}e^{-i(\alpha-\alpha_0)y}$ is the envelope function along the CCW direction. Results of this analysis are presented in Fig. 2(e) where we show the averaged waveguide power in the steady state $\langle |\psi^s|^2 \rangle = \int_L |\psi^s(y)|^2 dy$, in units of threshold, as a function of the laser detuning. When the laser frequency is red-shifted the intra-waveguide power start to increase until a clear series of discrete steps (see inset), decreasing the average power, are seen in the yellow area, which corresponds to the region where there is hysteresis in the system and the soliton solutions are expected to appear [11, 54]. In fact, these steps have been previously measured experimentally in the transmission of non-linear ring resonators, and they are associated to the formation of different soliton states within

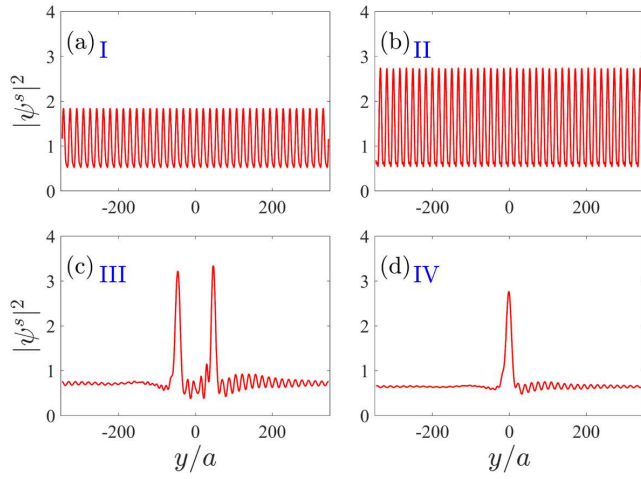


FIG. 3. Steady state envelope functions at the marked points I-IV in Fig. 2(e). (a) Supercritical Turing pattern with 40 rolls. (b) Supercritical Turing pattern with 41 rolls. (c) Soliton molecule of two pulses. (d) Single soliton pulse. $|\psi^s|^2$ is given in units of the power threshold $|\mathcal{A}_{\alpha_0}|_{\text{th}}^2$.

the system, in excellent agreement with the predictions of the non-linear coupled mode equations and the Lugiato-Lefever formalism [20]. We show in Figs. 2(f)-2(i) the respective frequency combs at the four representative points marked in Fig. 2(e). Figures 2(f) and 2(g) displays a sequence of primary combs separated by 40-FSR and 41-FSR, respectively, which correspond to supercritical Turing patterns as they are excited above threshold. In Figs. 2(h)-2(i), both combs are subcritical (excited right below threshold) with a single FSR spacing, and they are the signature of soliton complexes. Notably, because of the presence of non-trivial high order terms in the dispersion relation of the photonic crystal CCW, these frequency combs have signatures of dispersive wave formation or soliton Cherenkov radiation at the linear phase matching condition $\omega_\alpha - [\omega_{\alpha_0} + \zeta_1(\alpha - \alpha_0)] = 0$, where ζ_1 represents the group velocity [25]. Particularly, the dispersive peak closest to the zero comb line is predicted around $a\alpha \simeq 1.63$, which is in perfect agreement with our numerical simulations. The corresponding steady state intensity of the envelope functions are shown in Fig. 3. For the I (40 FSR repetition rate) and II (41 FSR repetition rate) states, we see 40 and 41 Turing rolls, respectively, in agreement with the Lugiato-Lefever theory of Kerr frequency combs in the anomalous dispersion regime [54]. Moreover, for the III and IV states we clearly identify, respectively, a soliton molecule composed of two pulses and a single soliton pulse, propagating along the waveguide direction while keeping their shape and amplitude. It must be said that because these soliton structures are subcritical (pumped below threshold), they are extremely sensitive to the initial conditions, and therefore, the system may follow different trajectories in Fig 2(e) when slightly changing the Bloch mode

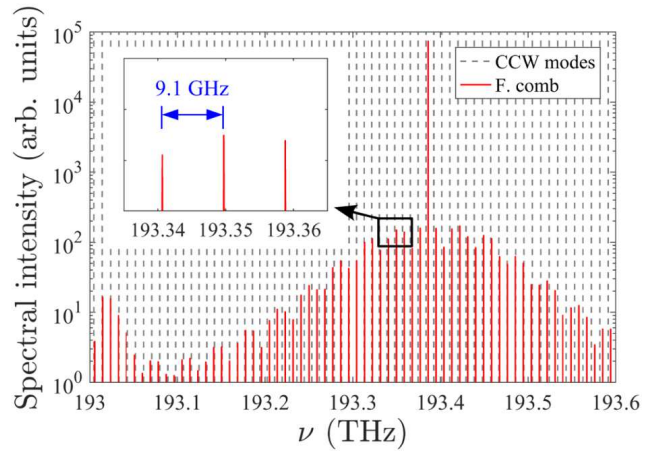


FIG. 4. Frequency spectrum of the DKS in Fig. 3(d), where the dashed vertical lines represent the normal modes of the photonic crystal CCW. A small repetition rate of 9.1 GHz is obtained.

amplitudes at $t = 0$ [20, 54]. Furthermore, the characteristic width of the soliton pulse is much smaller than the waveguide length thus ruling out finite-size effects in the basis expansion. While results presented in Fig. 2 are strictly valid for a CCW system with periodic boundary conditions, we still expect highly coherent combs in finite waveguides where non-negligible corrections to the non-linear interaction are predicted by the theory of frequency combs in Fabry-Perot resonators [30]. Nevertheless, a rigorous quantitative analysis is out of the scope of this paper, and will be focus of a future work.

Figure 4 shows the frequency spectrum of the DKS in Fig. 3(d), where the unloaded modes (normal modes of the CCW) are represented by the vertical dashed lines. As expected from energy conservation, the spectral lines are equally spaced with a repetition rate of 9.1 GHz. Such rates have been previously achieved in non-linear ring resonators of 7 mm diameter [55], in contrast to our system length of $\sim 277 \mu\text{m}$. Notice that the minimal external power for comb generation may significantly vary depending on the material, geometry and more importantly, the coupling architecture with a bus waveguide [46], however, this important result notably highlights the potential capabilities of μm -scale low-threshold CCW systems to generate low-rate frequency combs, which are desirable in high-precision comb applications [11].

It is important to stress that the specific choice of photonic crystal CCWs is mainly motivated by their characteristic diffraction-limited mode volumes [56] which play an important role on decreasing the threshold power and final device size. Nevertheless, the results presented in this section only rely on the dispersion relation of the CCW and are therefore expected for any CCW system, e.g. coupled microrings, displaying anomalous dispersion with, more generally, n -th neighbor coupling.

IV. CONCLUSIONS

In conclusion, we have presented results on Kerr frequency combs and DKS in CCWs where the main source of non-linear losses is given by TPA. We found that the internal mode threshold for comb generation depends on the main CCW figures of merit, namely, cavity volume, normal mode quality factor and group index. While TPA losses has the main effect of increasing the threshold power and inducing a red shift in the optimal laser detuning, structural slow-light plays an important role on reducing the minimal power to trigger FWM phenomena between the CCW normal modes, evidencing the capabilities of CCW systems for low-threshold frequency combs.

Specifically, we have demonstrated the possibility of DKS in a realistic dispersion-engineered silicon photonic crystal CCW at telecom wavelengths, where highly-complex combs were seen with signatures of soliton Cherenkov radiation. Repetition rates of few gigahertz in a $\sim 277 \mu\text{m}$ -length photonic crystal CCW have been obtained into the soliton regime, which are commonly achieved in $\sim 7 \text{ mm}$ size ring resonators, thus demonstrating the potential of CCW systems for high-precision comb applications in ultra-compact devices. Finally, although the spectral spanning of the combs generated in CCW is limited to the waveguide bandwidth, our results open the way to Kerr frequency comb and DKS generation via advanced dispersion engineering and slow-light non-linear enhancement.

Appendix A: Electromagnetic wave equation

We start from Maxwell's curl equations

$$\nabla \times \mathbf{E}(\mathbf{r}, t) + \mu_0 \frac{\partial \mathbf{H}(\mathbf{r}, t)}{\partial t} = 0 \quad (\text{A1})$$

$$\nabla \times \mathbf{H}(\mathbf{r}, t) - \epsilon_0 \epsilon(\mathbf{r}, |\mathbf{E}|^2) \frac{\partial \mathbf{E}(\mathbf{r}, t)}{\partial t} = 0, \quad (\text{A2})$$

where the material is assumed to be non-dispersive, non-linear and isotropic. If we apply the curl operator to Eq. A1 and then use Eq. A2 we get the wave equation for $\mathbf{E}(\mathbf{r}, t)$

$$\left[\hat{\mathcal{L}} + \frac{\epsilon(\mathbf{r}, |\mathbf{E}|^2)}{c^2} \frac{\partial^2}{\partial t^2} \right] \mathbf{E}(\mathbf{r}, t) = 0, \quad (\text{A3})$$

where $\hat{\mathcal{L}} = \nabla \times \nabla \times$ and $c = 1/\sqrt{\epsilon_0 \mu_0}$.

Appendix B: Electric field expansion

Because the absolute intensity of the electric field determines the effective strength of the Kerr non-linearity, it is very important to write $\mathbf{E}(\mathbf{r}, t)$ in proper units. We specifically adopt the SI system, where the electric field has units of [V/m], and expand it in terms of the normal modes of the coupled-cavities waveguide (CCW):

$$\mathbf{E}(\mathbf{r}, t) = \sum_{\mu} \mathcal{A}'_{\mu}(t) e^{-i\omega_{\mu} t} \mathbf{E}_{\mu}(\mathbf{r}) + E_{\text{ext}} e^{-i\Omega_0 t} \hat{e}_0, \quad (\text{B1})$$

where $\mathcal{A}'_{\mu}(t)$ is the slowly-varying amplitude of the normal mode $\mathbf{E}_{\mu}(\mathbf{r})$ with eigenfrequency ω_{μ} and momentum μ (along the waveguide direction $\hat{\mu}$), and E_{ext} is the electric field amplitude of the driving continuous-wave (cw) source with frequency Ω_0 and vector direction \hat{e}_0 . Equation B1 is the so called slowly-varying amplitude expansion, as the time and spatial variations have been separated, and the fast-varying temporal dependence is explicitly represented by the oscillatory term $e^{-i\omega_{\mu} t}$. Notice that the field $\mathbf{E}_{\mu}(\mathbf{r})$ in Eq. B1 also has units of [V/m], then \mathcal{A}' is dimensionless. In order to express the CCW normal modes in a more convenient form we write

$$\mathbf{E}_{\mu}(\mathbf{r}) = \sqrt{N_{\mu}} \vec{\mathcal{E}}_{\mu}(\mathbf{r}), \quad (\text{B2})$$

where N_{μ} is a normalization factor and $\vec{\mathcal{E}}_{\mu}(\mathbf{r})$ fulfills the generalized eigenvalue equation

$$\hat{\mathcal{L}} \vec{\mathcal{E}}_{\mu}(\mathbf{r}) = \frac{\tilde{\omega}_{\mu}^2}{c^2} \epsilon(\mathbf{r}) \vec{\mathcal{E}}_{\mu}(\mathbf{r}), \quad (\text{B3})$$

subject to the normalization condition

$$\int_l \epsilon(\mathbf{r}) \vec{\mathcal{E}}_\alpha^*(\mathbf{r}) \cdot \vec{\mathcal{E}}_\mu(\mathbf{r}) dV = \delta_{\alpha,\mu}, \quad (\text{B4})$$

with l representing the period of the waveguide and $\epsilon(\mathbf{r})$ its dielectric function. Equation B4 sets the units of $\vec{\mathcal{E}}_\mu(\mathbf{r})$ to $[\text{m}^{-3/2}]$. In Eq. B3 we have considered the complex frequency

$$\tilde{\omega}_\mu = \omega_\mu - i\frac{\gamma_\mu}{2}, \quad (\text{B5})$$

where γ_μ is the overall loss rate of the Bloch mode $\vec{\mathcal{E}}_\mu(\mathbf{r})$. For the particular case of a photonic crystal slab, γ_μ represents the out-of-plane losses due to the coupling with the leaky modes of the homogeneous system [41]. Notice that the normalization condition of Eq. B4, satisfied by normal modes, is not rigorously valid when the eigenvalue of Eq. B3 is complex, i.e., when dealing with quasinormal modes [56]. Nevertheless it still represents a very good approximation in the low loss limit $\gamma_\mu \ll \omega_\mu$, which is the case of interest in the present formulation. The normalization factor N_μ can be easily found by recalling the fundamental relation between the group velocity $v_g(\mu)$, averaged energy flux and averaged energy density of the electromagnetic field, which holds in periodic waveguides [57]

$$v_g(\mu) = \frac{\int_l \hat{\mu} \cdot \mathbf{S}_\mu dV}{\mathcal{U}_{\mathbf{E}_\mu} + \mathcal{U}_{\mathbf{H}_\mu}}, \quad (\text{B6})$$

where $\mathbf{S}_\mu(\mathbf{r}) = \text{Re}[\mathbf{E}_\mu^*(\mathbf{r}) \times \mathbf{H}_\mu(\mathbf{r})]/2$ is the time-averaged Poynting vector (energy flux), $\mathcal{U}_{\mathbf{E}_\mu} = \int_l \epsilon_0 \epsilon(\mathbf{r}) |\mathbf{E}_\mu(\mathbf{r})|^2 dV/4$ is the physical electric field energy (integrated density energy) and $\mathcal{U}_{\mathbf{H}_\mu} = \int_l \mu_0 |\mathbf{H}_\mu(\mathbf{r})|^2 dV/4$ the magnetic one in the waveguide period. If we set the waveguide direction along the y axis, i.e., $\hat{\mu} = \hat{y}$, and use the result that for harmonic modes the electric and magnetic field energies are equal [57], i.e., $\mathcal{U}_{\mathbf{E}_\mu} = \mathcal{U}_{\mathbf{H}_\mu}$, Eq. B6 takes the following form

$$v_g(\mu) = \frac{\int_l dy \left[\int_\infty dx dz S_{\mu,y} \right]}{2\mathcal{U}_{\mathbf{E}_\mu}}, \quad (\text{B7})$$

where the last integral is carried out over all space and it is the power flux $P_\mu = \int_\infty dx dz S_{\mu,y}$ through the transverse cross section of the waveguide, which has been shown to be independent of y [43], therefore

$$v_g(\mu) = \frac{lP_\mu}{2\mathcal{U}_{\mathbf{E}_\mu}}. \quad (\text{B8})$$

Using the definition of $\mathcal{U}_{\mathbf{E}_\mu}$, Eq. B8 turns into

$$v_g(\mu) = \frac{lP_\mu}{\frac{1}{2} \int_l \epsilon_0 \epsilon(\mathbf{r}) |\mathbf{E}_\mu(\mathbf{r})|^2 dV}, \quad (\text{B9})$$

which means that the electric field $\mathbf{E}_\mu(\mathbf{r})$ must fulfill

$$\int_l \epsilon(\mathbf{r}) |\mathbf{E}_\mu(\mathbf{r})|^2 dV = \frac{2lP_\mu}{\epsilon_0 v_g(\mu)}. \quad (\text{B10})$$

The expression for N_μ is readily found from Eqs. B2, B4 and B10

$$N_\mu = \frac{2lP_\mu}{\epsilon_0 v_g(\mu)}, \quad (\text{B11})$$

and the field expansion in Eq. B1 is thus expressed in terms of the electric field eigenmodes $\vec{\mathcal{E}}_\mu(\mathbf{r})$ as follows

$$\mathbf{E}(\mathbf{r}, t) = \sqrt{\frac{2l}{\epsilon_0}} \sum_\mu \sqrt{P_\mu} \mathcal{A}'_\mu(t) e^{-i\omega_\mu t} \frac{1}{\sqrt{v_g(\mu)}} \vec{\mathcal{E}}_\mu(\mathbf{r}) + E_{\text{ext}} e^{-i\Omega_0 t} \hat{e}_0. \quad (\text{B12})$$

We now define the new amplitude $\mathcal{A}_\mu(t) = \sqrt{P_\mu} \mathcal{A}'_\mu(t)$ and simplify the notation for the group velocity of the mode μ as $v_g(\mu) \rightarrow v_\mu$. The electric field expansion takes the following final form

$$\mathbf{E}(\mathbf{r}, t) = \sqrt{\frac{2l}{\epsilon_0}} \sum_\mu \mathcal{A}_\mu(t) e^{-i\omega_\mu t} \frac{1}{\sqrt{v_\mu}} \vec{\mathcal{E}}_\mu(\mathbf{r}) + E_{\text{ext}} e^{-i\Omega_0 t} \hat{e}_0, \quad (\text{B13})$$

where $|\mathcal{A}_\mu(t)|^2$ is the instantaneous power, in [W] units, of the mode μ propagating in the waveguide direction.

Appendix C: Non-linear coupled mode equations

Let's now consider a CCW of M cavities where the total electric field of the system is represented by Eq. B13 and the normalization condition of Eq. B4 is written as

$$\int_L \epsilon(\mathbf{r}) \vec{\mathcal{E}}_\alpha^*(\mathbf{r}) \cdot \vec{\mathcal{E}}_\mu(\mathbf{r}) dV = M \delta_{\alpha,\mu}, \quad (\text{C1})$$

when integrating over the total waveguide length $L = Ml$. The second time-derivative of Eq. B13 reads

$$\frac{\partial^2 \mathbf{E}(\mathbf{r}, t)}{\partial t^2} = \sqrt{\frac{2l}{\epsilon_0}} \sum_\mu \left[\ddot{\mathcal{A}}_\mu(t) - 2i\omega_\mu \dot{\mathcal{A}}_\mu(t) - \omega_\mu^2 \mathcal{A}_\mu(t) \right] e^{-i\omega_\mu t} \frac{1}{\sqrt{v_\mu}} \vec{\mathcal{E}}_\mu(\mathbf{r}) - \Omega_0^2 E_{\text{ext}} e^{-i\Omega_0 t} \hat{e}_0, \quad (\text{C2})$$

while the operator $\hat{\mathcal{L}}$ applied to Eq. B13 gives

$$\hat{\mathcal{L}} \mathbf{E}(\mathbf{r}, t) = \sqrt{\frac{2l}{\epsilon_0}} \frac{1}{c^2} \sum_\mu \tilde{\omega}_\mu^2 \mathcal{A}_\mu(t) e^{-i\omega_\mu t} \frac{1}{\sqrt{v_\mu}} \epsilon(\mathbf{r}) \vec{\mathcal{E}}_\mu(\mathbf{r}), \quad (\text{C3})$$

where we have used Eq. B3. Because $\mathbf{E}(\mathbf{r}, t)$ must satisfy the wave equation in Eq. A3, we employ Eqs. C2 and C3 to get

$$\begin{aligned} & \sum_\mu \tilde{\omega}_\mu^2 \mathcal{A}_\mu(t) e^{-i\omega_\mu t} \frac{1}{\sqrt{v_\mu}} \epsilon(\mathbf{r}) \vec{\mathcal{E}}_\mu(\mathbf{r}) \\ & + \epsilon(\mathbf{r}, |\mathbf{E}|^2) \left\{ \sum_\mu \left[\ddot{\mathcal{A}}_\mu(t) - 2i\omega_\mu \dot{\mathcal{A}}_\mu(t) - \omega_\mu^2 \mathcal{A}_\mu(t) \right] e^{-i\omega_\mu t} \frac{1}{\sqrt{v_\mu}} \vec{\mathcal{E}}_\mu(\mathbf{r}) - \sqrt{\frac{\epsilon_0}{2l}} \Omega_0^2 E_{\text{ext}} e^{-i\Omega_0 t} \hat{e}_0 \right\} = 0. \end{aligned} \quad (\text{C4})$$

The intensity dependent dielectric function in Eq. C4 can be set to the reference value $\epsilon(\mathbf{r}) = \epsilon(\mathbf{r}, 0)$ in the pump contribution as the perturbation induced by $|\mathbf{E}|^2$ can be neglected when driving the system at $\epsilon(\mathbf{r})$. Therefore, Eq. C4 turns into

$$\begin{aligned} & \sum_\mu \tilde{\omega}_\mu^2 \mathcal{A}_\mu(t) e^{-i\omega_\mu t} \frac{1}{\sqrt{v_\mu}} \epsilon(\mathbf{r}) \vec{\mathcal{E}}_\mu(\mathbf{r}) \\ & + \epsilon(\mathbf{r}, |\mathbf{E}|^2) \sum_\mu \left[\ddot{\mathcal{A}}_\mu(t) - 2i\omega_\mu \dot{\mathcal{A}}_\mu(t) - \omega_\mu^2 \mathcal{A}_\mu(t) \right] e^{-i\omega_\mu t} \frac{1}{\sqrt{v_\mu}} \vec{\mathcal{E}}_\mu(\mathbf{r}) - \epsilon(\mathbf{r}) \sqrt{\frac{\epsilon_0}{2l}} \Omega_0^2 E_{\text{ext}} e^{-i\Omega_0 t} \hat{e}_0 = 0. \end{aligned} \quad (\text{C5})$$

At this point we explicitly write the intensity dependent dielectric function as [58]

$$\epsilon(\mathbf{r}, |\mathbf{E}|^2) = \left[n(\mathbf{r}) + n_2(\mathbf{r}) I(\mathbf{r}, |\mathbf{E}|^2) + i \frac{c}{2\omega_0} \beta_{\text{TPA}}(\mathbf{r}) I(\mathbf{r}, |\mathbf{E}|^2) \right]^2, \quad (\text{C6})$$

where $n(\mathbf{r}) = \sqrt{\epsilon(\mathbf{r})}$ is the linear refractive index, $n_2(\mathbf{r})$ and $\beta_{\text{TPA}}(\mathbf{r})$ are the spatial dependent Kerr and two-photon absorption (TPA) coefficients, respectively, of the material at ω_0 and

$$I(\mathbf{r}, |\mathbf{E}|^2) = \frac{\epsilon_0 c}{2} n(\mathbf{r}) |\mathbf{E}|^2, \quad (\text{C7})$$

is the instantaneous electric field intensity. As the non-linear shift induced on the dielectric function is expected to be small, Eq. C6 can be approximated to

$$\epsilon(\mathbf{r}, |\mathbf{E}|^2) \simeq \epsilon(\mathbf{r}) + 2n(\mathbf{r}) \Delta n(\mathbf{r}, |\mathbf{E}|^2), \quad (\text{C8})$$

with

$$\Delta n(\mathbf{r}, |\mathbf{E}|^2) = \frac{\epsilon_0 c}{2} n(\mathbf{r}) \left[n_2(\mathbf{r}) + i \frac{c}{2\omega_0} \beta_{\text{TPA}}(\mathbf{r}) \right] |\mathbf{E}|^2. \quad (\text{C9})$$

Replacing Eq. C8 in Eq. C5 gives (after reorganizing terms)

$$\begin{aligned}
& \sum_{\mu} (\tilde{\omega}_{\mu}^2 - \omega_{\mu}^2) \mathcal{A}_{\mu}(t) e^{-i\omega_{\mu}t} \frac{1}{\sqrt{v_{\mu}}} \epsilon(\mathbf{r}) \vec{\mathcal{E}}_{\mu}(\mathbf{r}) + \sum_{\mu} \left[\ddot{\mathcal{A}}_{\mu}(t) - 2i\omega_{\mu} \dot{\mathcal{A}}_{\mu}(t) \right] e^{-i\omega_{\mu}t} \frac{1}{\sqrt{v_{\mu}}} \epsilon(\mathbf{r}) \vec{\mathcal{E}}_{\mu}(\mathbf{r}) \\
& - 2 \sum_{\mu} \omega_{\mu}^2 \mathcal{A}_{\mu}(t) e^{-i\omega_{\mu}t} \frac{1}{\sqrt{v_{\mu}}} n(\mathbf{r}) \Delta n(\mathbf{r}, |\mathbf{E}|^2) \vec{\mathcal{E}}_{\mu}(\mathbf{r}) \\
& + 2 \sum_{\mu} \left[\ddot{\mathcal{A}}_{\mu}(t) - 2i\omega_{\mu} \dot{\mathcal{A}}_{\mu}(t) \right] e^{-i\omega_{\mu}t} \frac{1}{\sqrt{v_{\mu}}} n(\mathbf{r}) \Delta n(\mathbf{r}, |\mathbf{E}|^2) \vec{\mathcal{E}}_{\mu}(\mathbf{r}) - \epsilon(\mathbf{r}) \sqrt{\frac{\epsilon_0}{2l}} \Omega_0^2 E_{\text{ext}} e^{-i\Omega_0 t} \hat{e}_0 = 0. \quad (\text{C10})
\end{aligned}$$

In order to arrive to a system of differential equations for the slowly-varying amplitudes, Eq. C10 is multiplied by $\vec{\mathcal{E}}_{\alpha}^*(\mathbf{r})$ and integrated over the whole waveguide. After the orthogonality condition of Eq. C1 is explicitly applied, we get

$$\begin{aligned}
& (\tilde{\omega}_{\alpha}^2 - \omega_{\alpha}^2) \mathcal{A}_{\alpha}(t) e^{-i\omega_{\alpha}t} \frac{1}{\sqrt{v_{\alpha}}} + \left[\ddot{\mathcal{A}}_{\alpha}(t) - 2i\omega_{\alpha} \dot{\mathcal{A}}_{\alpha}(t) \right] e^{-i\omega_{\alpha}t} \frac{1}{\sqrt{v_{\alpha}}} \\
& - \frac{2}{M} \sum_{\mu} \omega_{\mu}^2 \mathcal{A}_{\mu}(t) e^{-i\omega_{\mu}t} \frac{1}{\sqrt{v_{\mu}}} \int_L n(\mathbf{r}) \Delta n(\mathbf{r}, |\mathbf{E}|^2) \vec{\mathcal{E}}_{\alpha}^*(\mathbf{r}) \cdot \vec{\mathcal{E}}_{\mu}(\mathbf{r}) dV \\
& + \frac{2}{M} \sum_{\mu} \left[\ddot{\mathcal{A}}_{\mu}(t) - 2i\omega_{\mu} \dot{\mathcal{A}}_{\mu}(t) \right] e^{-i\omega_{\mu}t} \frac{1}{\sqrt{v_{\mu}}} \int_L n(\mathbf{r}) \Delta n(\mathbf{r}, |\mathbf{E}|^2) \vec{\mathcal{E}}_{\alpha}^*(\mathbf{r}) \cdot \vec{\mathcal{E}}_{\mu}(\mathbf{r}) dV \\
& - \sqrt{\frac{\epsilon_0}{2l}} \Omega_0^2 E_{\text{ext}} e^{-i\Omega_0 t} \int_l \epsilon(\mathbf{r}) \vec{\mathcal{E}}_{\alpha}^*(\mathbf{r}) \cdot \hat{e}_0 dV = 0. \quad (\text{C11})
\end{aligned}$$

We now apply the slowly-varying assumption where the second derivative terms are assumed to be small, i.e., $|\ddot{\mathcal{A}}_{\alpha}(t)| \ll |2\omega_{\alpha} \dot{\mathcal{A}}_{\alpha}(t)|$, and consequently they can be neglected, as well as the first derivative term multiplying the non-linear perturbation $\Delta n(\mathbf{r}, |\mathbf{E}|^2)$ in the second integral of Eq. C11. We also assume low-loss CCWs, for which we can approximate $\tilde{\omega}_{\alpha}^2 - \omega_{\alpha}^2 \simeq -i\omega_{\alpha} \gamma_{\alpha}$ in the first term of the equation. Therefore, Eq. C11 is rewritten as

$$\dot{\mathcal{A}}_{\alpha}(t) e^{-i\omega_{\alpha}t} + \frac{\gamma_{\alpha}}{2} \mathcal{A}_{\alpha}(t) e^{-i\omega_{\alpha}t} - \frac{i\sqrt{v_{\alpha}}}{\omega_{\alpha} M} \sum_{\mu} \omega_{\mu}^2 \mathcal{A}_{\mu}(t) e^{-i\omega_{\mu}t} \frac{1}{\sqrt{v_{\mu}}} \int_L n(\mathbf{r}) \Delta n(\mathbf{r}, |\mathbf{E}|^2) \vec{\mathcal{E}}_{\alpha}^*(\mathbf{r}) \cdot \vec{\mathcal{E}}_{\mu}(\mathbf{r}) dV - \frac{\gamma_{\alpha}}{2} \mathcal{F}_{\alpha} e^{-i\Omega_0 t} = 0 \quad (\text{C12})$$

where we have defined the driving amplitude

$$\mathcal{F}_{\alpha} = \frac{i\Omega_0^2}{\omega_{\alpha} \gamma_{\alpha}} \sqrt{\frac{\epsilon_0 v_{\alpha}}{2l}} E_{\text{ext}} \int_l \epsilon(\mathbf{r}) \vec{\mathcal{E}}_{\alpha}^*(\mathbf{r}) \cdot \hat{e}_0 dV. \quad (\text{C13})$$

Let's focus on the non-linear term of Eq. C12. From the field expansion in Eq. B13, the intra-waveguide modulus squared field is given by

$$|\mathbf{E}(\mathbf{r}, t)|^2 = \frac{2l}{\epsilon_0} \sum_{\eta\xi} \mathcal{A}_{\eta}^*(t) e^{i\omega_{\eta}t} \mathcal{A}_{\xi}(t) e^{-i\omega_{\xi}t} \frac{1}{\sqrt{v_{\eta}v_{\xi}}} \vec{\mathcal{E}}_{\eta}^*(\mathbf{r}) \cdot \vec{\mathcal{E}}_{\xi}(\mathbf{r}), \quad (\text{C14})$$

therefore, the non-linear perturbation in Eq. C9 is written as

$$\Delta n(\mathbf{r}, |\mathbf{E}|^2) = lc \sum_{\eta\xi} \mathcal{A}_{\eta}^*(t) e^{i\omega_{\eta}t} \mathcal{A}_{\xi}(t) e^{-i\omega_{\xi}t} \frac{1}{\sqrt{v_{\eta}v_{\xi}}} n(\mathbf{r}) \left[n_2(\mathbf{r}) + i\frac{c}{2\omega_0} \beta_{\text{TPA}}(\mathbf{r}) \right] \vec{\mathcal{E}}_{\eta}^*(\mathbf{r}) \cdot \vec{\mathcal{E}}_{\xi}(\mathbf{r}), \quad (\text{C15})$$

and the integral of Eq. C12 becomes

$$\int_L n(\mathbf{r}) \Delta n(\mathbf{r}, |\mathbf{E}|^2) \vec{\mathcal{E}}_{\alpha}^*(\mathbf{r}) \cdot \vec{\mathcal{E}}_{\mu}(\mathbf{r}) dV = lc \sum_{\eta\xi} \mathcal{A}_{\eta}^*(t) e^{i\omega_{\eta}t} \mathcal{A}_{\xi}(t) e^{-i\omega_{\xi}t} \frac{1}{\sqrt{v_{\eta}v_{\xi}}} \int_L \tilde{n}_2(\mathbf{r}) \epsilon(\mathbf{r}) \left[\vec{\mathcal{E}}_{\alpha}^*(\mathbf{r}) \cdot \vec{\mathcal{E}}_{\mu}(\mathbf{r}) \right] \left[\vec{\mathcal{E}}_{\eta}^*(\mathbf{r}) \cdot \vec{\mathcal{E}}_{\xi}(\mathbf{r}) \right] dV, \quad (\text{C16})$$

where we have defined the complex Kerr coefficient

$$\tilde{n}_2(\mathbf{r}) = n_2(\mathbf{r}) + i\frac{c}{2\omega_0} \beta_{\text{TPA}}(\mathbf{r}). \quad (\text{C17})$$

In order to write the last integral term of Eq. C16 in a more convenient form, we assume that the normal modes of the CCW can be expanded in the cavity mode basis

$$\vec{\mathcal{E}}_\mu(\mathbf{r}) = \sum_m C_m(\mu) \vec{\Upsilon}_m(\mathbf{r}), \quad (\text{C18})$$

which is a very good approximation as long as the modes are strongly confined in the cavity region [59]. In Eq. C18, $\vec{\Upsilon}_m(\mathbf{r})$ is the eigenmode of the m -th cavity in units of $[\text{m}^{-3/2}]$ and normalized as

$$\int_\infty \epsilon_c(\mathbf{r}) |\vec{\Upsilon}_m(\mathbf{r})|^2 dV = 1, \quad (\text{C19})$$

with $\epsilon_c(\mathbf{r})$ being the dielectric function of the single cavity system. By replacing Eq. C18 into Eq. C16, the non-linear integral can be rewritten as

$$\int_L n(\mathbf{r}) \Delta n(\mathbf{r}, |\mathbf{E}|^2) \vec{\mathcal{E}}_\alpha^*(\mathbf{r}) \cdot \vec{\mathcal{E}}_\mu(\mathbf{r}) dV = lc \sum_{\eta\xi} \mathcal{A}_\eta^*(t) e^{i\omega_\eta t} \mathcal{A}_\xi(t) e^{-i\omega_\xi t} \frac{1}{\sqrt{v_\eta v_\xi}} \sum_{lmhp} C_l^*(\alpha) C_m(\mu) C_h^*(\eta) C_p(\xi) \Pi_{lmhp}, \quad (\text{C20})$$

where the non-linear overlapping elements Π_{lmhp} are given by

$$\Pi_{lmhp} = \int_L \tilde{n}_2(\mathbf{r}) \epsilon(\mathbf{r}) \left[\vec{\Upsilon}_l^*(\mathbf{r}) \cdot \vec{\Upsilon}_m(\mathbf{r}) \right] \left[\vec{\Upsilon}_h^*(\mathbf{r}) \cdot \vec{\Upsilon}_p(\mathbf{r}) \right] dV. \quad (\text{C21})$$

Since the mode $\vec{\Upsilon}_m(\mathbf{r})$ is strongly confined in the cavity region, the Kerr shift on cavity m induced by the field of neighbor cavities ($m \pm 1, m \pm 2, \dots$), is expected to be very small in comparison to the shift induced by its own field strength, therefore, we can safely neglect the cross-Kerr terms in Eq. C21 and consider only the diagonal one in the sum of Eq. C20, i.e.,

$$\int_L n(\mathbf{r}) \Delta n(\mathbf{r}, |\mathbf{E}|^2) \vec{\mathcal{E}}_\alpha^*(\mathbf{r}) \cdot \vec{\mathcal{E}}_\mu(\mathbf{r}) dV \simeq lc \sum_{\eta\xi} \mathcal{A}_\eta^*(t) e^{i\omega_\eta t} \mathcal{A}_\xi(t) e^{-i\omega_\xi t} \frac{1}{\sqrt{v_\eta v_\xi}} \sum_m C_m^*(\alpha) C_m(\mu) C_m^*(\eta) C_m(\xi) \Pi_m, \quad (\text{C22})$$

with

$$\Pi_m = \int_L \tilde{n}_2(\mathbf{r}) \epsilon(\mathbf{r}) |\vec{\Upsilon}_m(\mathbf{r})|^4 dV. \quad (\text{C23})$$

Furthermore, the coefficient $\tilde{n}_2(\mathbf{r})$ is non-zero only within the non-linear material, which allow us to write Eq. C23 as

$$\Pi_m = \tilde{n}_2 \epsilon \int_L \Theta(\mathbf{r}) |\vec{\Upsilon}_m(\mathbf{r})|^4 dV. \quad (\text{C24})$$

where \tilde{n}_2 is the same of Eq. C17 but with no spatial dependence, ϵ is the dielectric constant of the non-linear material, and the function $\Theta(\mathbf{r})$ is defined as

$$\Theta(\mathbf{r}) = \begin{cases} 1 & \text{non-linear material} \\ 0 & \text{elsewhere} \end{cases} \quad (\text{C25})$$

In order to write Eq. C24 in a more intuitive way, it is an excellent approximation to express the integral of $|\vec{\Upsilon}_m(\mathbf{r})|^4$ in terms of the cavity non-linear mode volume V_m as follows

$$V_m = \frac{\left[\int_\infty \epsilon_c(\mathbf{r}) |\vec{\Upsilon}_m(\mathbf{r})|^2 dV \right]^2}{\int_\infty \epsilon_c^2(\mathbf{r}) |\vec{\Upsilon}_m(\mathbf{r})|^4 dV} = \frac{1}{\int_\infty \epsilon_c^2(\mathbf{r}) |\vec{\Upsilon}_m(\mathbf{r})|^4 dV} \simeq \frac{1}{\epsilon^2 \int_L \Theta(\mathbf{r}) |\vec{\Upsilon}_m(\mathbf{r})|^4 dV}. \quad (\text{C26})$$

Therefore

$$\Pi_m \simeq \frac{\tilde{n}_2}{\epsilon V_m}. \quad (\text{C27})$$

Using Eqs. C22 and C27 the system of Eq. C12 can be written as

$$\begin{aligned} & \dot{\mathcal{A}}_\alpha(t)e^{i\sigma_\alpha t} + \frac{\gamma_\alpha}{2}\mathcal{A}_\alpha(t)e^{i\sigma_\alpha t} \\ & - \frac{i\sqrt{v_\alpha}lc\tilde{n}_2}{\omega_\alpha\epsilon M} \sum_{\mu\eta\xi} \omega_\mu^2 \mathcal{A}_\mu(t)e^{i\sigma_\mu t} \mathcal{A}_\eta^*(t)e^{-i\sigma_\eta t} \mathcal{A}_\xi(t)e^{i\sigma_\xi t} \frac{1}{\sqrt{v_\mu v_\eta v_\xi}} \sum_m \frac{1}{V_m} C_m^*(\alpha) C_m(\mu) C_m^*(\eta) C_m(\xi) \\ & - \frac{\gamma_\alpha}{2} \mathcal{F}_\alpha \delta_{\alpha,\alpha_0} = 0, \end{aligned} \quad (\text{C28})$$

where we have introduced the frequency detuning of the mode μ with respect to the cw frequency Ω_0

$$\sigma_\mu = \Omega_0 - \omega_\mu, \quad (\text{C29})$$

and explicitly written the resonance condition for the driven term, which excites only the normal mode α_0 whose eigenfrequency is closest to the laser frequency Ω_0 . The explicit time dependence of Eq. C28 can be removed by carrying out the following transformation

$$\mathcal{B}_\mu(t) = \mathcal{A}_\mu(t)e^{i\sigma_\mu t}, \quad (\text{C30})$$

which turns Eq. C28 into

$$\dot{\mathcal{B}}_\alpha(t) + \left[\frac{\gamma_\alpha}{2} - i\sigma_\alpha \right] \mathcal{B}_\alpha(t) - \frac{i\sqrt{v_\alpha}lc\tilde{n}_2}{\omega_\alpha\epsilon M} \sum_{\mu\eta\xi} \frac{\omega_\mu^2 \mathcal{B}_\mu(t) \mathcal{B}_\eta^*(t) \mathcal{B}_\xi(t)}{\sqrt{v_\mu v_\eta v_\xi}} \sum_m \frac{1}{V_m} C_m^*(\alpha) C_m(\mu) C_m^*(\eta) C_m(\xi) - \frac{\gamma_\alpha}{2} \mathcal{F}_\alpha \delta_{\alpha,\alpha_0} = 0 \quad (\text{C31})$$

Equation C31 dictates the non-linear dynamics of the slowly-varying normal mode amplitudes in a CCW system with different coupled cavities, and no particular choice on the boundary conditions. This equation can be highly simplified if we consider identical single mode cavities and periodic boundary conditions, in which the expansion coefficients in the cavity basis are analytical [32]

$$C_m(\mu) = e^{-iml\mu}, \quad (\text{C32})$$

allowing to evaluate the second sum in Eq. C31

$$\sum_m \frac{1}{V_m} C_m^*(\alpha) C_m(\mu) C_m^*(\eta) C_m(\xi) = \frac{1}{V_c} \sum_m e^{-iml(\mu-\alpha+\xi-\eta)} = \frac{1}{V_c} \frac{\sin[(\mu-\alpha+\xi-\eta)Ml/2]}{\sin[(\mu-\alpha+\xi-\eta)l/2]} \simeq \frac{M}{V_c} \delta_{\xi,\alpha+\eta-\mu} \quad (\text{C33})$$

where V_c represents the cavity non-linear mode volume and the last approximation is valid for large M . Physically, the δ term in Eq. C33 represents the momentum conservation which is naturally expected from the periodic boundary condition assumption. Using this result, Eq. C31 takes the following form

$$\dot{\mathcal{B}}_\alpha(t) + \left[\frac{\gamma_\alpha}{2} - i\sigma_\alpha \right] \mathcal{B}_\alpha(t) - \frac{i\sqrt{v_\alpha}lc\tilde{n}_2}{\omega_\alpha\epsilon V_c} \sum_{\mu\eta} \frac{\omega_\mu^2 \mathcal{B}_\mu(t) \mathcal{B}_\eta^*(t) \mathcal{B}_{\alpha+\eta-\mu}(t)}{\sqrt{v_\mu v_\eta v_{\alpha+\eta-\mu}}} - \frac{\gamma_\alpha}{2} \mathcal{F}_\alpha \delta_{\alpha,\alpha_0} = 0. \quad (\text{C34})$$

Equation C34 can be further simplified by assuming that the strength of the non-linearity mainly depends on the frequency at which the non-linear effect takes place, $\omega_\alpha = \omega_{\alpha_0}$, and not on the frequencies contributing to the non-linear dynamics. This allows us to set the frequencies in the non-linear term to ω_{α_0} (frequency of the driven mode) as well as the group velocity terms to v_{α_0} . When the different frequencies are not independent and fulfill the energy conservation $\omega_\alpha + \omega_\eta = \omega_\mu + \omega_{\alpha+\eta-\mu}$, which is our case of interest, such approximation is expected to describe the non-linear phenomena accurately [60]. Equation C34 is thus turned into the following simpler expression

$$\dot{\mathcal{B}}_\alpha(t) + \left[\frac{\gamma_\alpha}{2} - i\sigma_\alpha \right] \mathcal{B}_\alpha(t) - \frac{i\omega_{\alpha_0} n_{g,\alpha_0} \tilde{n}_2}{\epsilon V_c} \sum_{\mu\eta} \mathcal{B}_\mu(t) \mathcal{B}_\eta^*(t) \mathcal{B}_{\alpha+\eta-\mu}(t) - \frac{\gamma_\alpha}{2} \mathcal{F}_\alpha \delta_{\alpha,\alpha_0} = 0, \quad (\text{C35})$$

where $n_{g,\alpha_0} = c/v_{\alpha_0}$ is the group index at ω_{α_0} . If we define the complex gain as

$$G_{\alpha_0} = g_{\alpha_0} + ig_{\alpha_0}^{\text{TPA}} \quad (\text{C36})$$

with

$$g_{\alpha_0} = \frac{l\omega_{\alpha_0} n_{g,\alpha_0} n_2}{\epsilon V_c}, \quad (\text{C37})$$

being the real gain coming from the non-linear Kerr effect, and

$$g_{\alpha_0}^{\text{TPA}} = \frac{lc n_{g,\alpha_0} \beta_{\text{TPA}}}{2\epsilon V_c}, \quad (\text{C38})$$

being the *imaginary gain*, representing the non-linear losses coming from TPA, we finally get the non-linear system of equations for the mode slowly-varying normal mode amplitudes in a CCW, with identical single mode cavities and periodic boundary conditions

$$\dot{\mathcal{B}}_{\alpha}(t) + \left[\frac{\gamma_{\alpha}}{2} - i\sigma_{\alpha} \right] \mathcal{B}_{\alpha}(t) - iG_{\alpha_0} \sum_{\mu\eta} \mathcal{B}_{\mu}(t) \mathcal{B}_{\eta}^*(t) \mathcal{B}_{\alpha+\eta-\mu}(t) - \frac{\gamma_{\alpha}}{2} \mathcal{F}_{\alpha} \delta_{\alpha,\alpha_0} = 0. \quad (\text{C39})$$

Equation C39 is equivalent to the one previously derived by Chembo and Yu in non-linear ring resonators [48].

Appendix D: Stationary solution and stability analysis

In order to simplify the analysis of the stationary solutions of Eq. C39 and their stability we introduce shifted momentum indices $\{\alpha', \mu', \eta'\} \rightarrow \{\alpha, \mu, \eta\} - \alpha_0$, where the driven mode has zero index and the side modes are symmetrically distributed around the driven one. In terms of this new indexes Eq. C39 is written as

$$\dot{\mathcal{B}}_{\alpha'}(t) + \left[\frac{\gamma_{\alpha'}}{2} - i\sigma_{\alpha'} \right] \mathcal{B}_{\alpha'}(t) - iG_0 \sum_{\mu'\eta'} \mathcal{B}_{\mu'}(t) \mathcal{B}_{\eta'}^*(t) \mathcal{B}_{\alpha'+\eta'-\mu'}(t) - \frac{\gamma_{\alpha'}}{2} \mathcal{F}_{\alpha'} \delta_{\alpha',0} = 0. \quad (\text{D1})$$

1. Stationary solution

The stationary solution of Eq. D1 is found by setting the derivative term to zero

$$\left[\frac{\gamma_{\alpha'}}{2} - i\sigma_{\alpha'} \right] \mathcal{B}_{\alpha'}^s - iG_0 \sum_{\mu'\eta'} \mathcal{B}_{\mu'}^s \mathcal{B}_{\eta'}^{s*} \mathcal{B}_{\alpha'+\eta'-\mu'}^s - \frac{\gamma_{\alpha'}}{2} \mathcal{F}_{\alpha'} \delta_{\alpha',0} = 0. \quad (\text{D2})$$

2. System below threshold

When the system is below threshold only the $\alpha' = 0$ mode is excited, then, Eq. D2 becomes

$$\frac{\gamma_0}{2} \mathcal{B}_0^s - i\sigma_0 \mathcal{B}_0^s - iG_0 |\mathcal{B}_0^s|^2 \mathcal{B}_0^s - \frac{\gamma_0}{2} \mathcal{F}_0 = 0, \quad (\text{D3})$$

and we get the very well known cubic relation between $|\mathcal{F}_0|^2$ and $|\mathcal{B}_0^s|^2$ which leads to the hysteresis phenomenon and bistability of the stationary solution

$$|\mathcal{F}_0|^2 = \left(1 + \frac{4\sigma_0^2}{\gamma_0^2} \right) |\mathcal{B}_0^s|^2 + \frac{4}{\gamma_0} \left(\frac{2g_0\sigma_0}{\gamma_0} + g_0^{\text{TPA}} \right) |\mathcal{B}_0^s|^4 + \frac{4|G_0|^2}{\gamma_0^2} |\mathcal{B}_0^s|^6. \quad (\text{D4})$$

The bistability boundaries B_{\pm} correspond to the local extrema of Eq. D4, which are the solutions of the quadratic equation $\partial|\mathcal{F}_0|^2/\partial|\mathcal{B}_0^s|^2 = 0$ on $|\mathcal{B}_0^s|^2$. Thus, we readily obtain

$$B_{\pm} = \frac{-(2\sigma_0 g_0 + \gamma_0 g_0^{\text{TPA}}) \pm \frac{1}{2} \sqrt{4(2\sigma_0 g_0 + \gamma_0 g_0^{\text{TPA}})^2 - 3|G_0|^2(4\sigma_0^2 + \gamma_0^2)}}{3|G_0|^2}. \quad (\text{D5})$$

Hysteresis exists if the boundaries B_{\pm} are real and positive, implying the following condition on the laser detuning

$$\sigma_0 < \sigma_{\text{hyst}} \rho(\kappa), \quad (\text{D6})$$

where

$$\sigma_{\text{hyst}} = -\frac{\gamma_0 \sqrt{3}}{2}, \quad (\text{D7})$$

and $\rho(\kappa)$ is a function which depends on the material properties only

$$\rho(\kappa) = \frac{(4\sqrt{3} + 3\kappa)\kappa + 3}{3(1 - 3\kappa^2)}, \quad (\text{D8})$$

with the dimensionless parameter κ defined as

$$\kappa = \frac{g_0^{\text{TPA}}}{g_0} = \frac{c\beta_{\text{TPA}}}{2n_2\omega_0}. \quad (\text{D9})$$

Notice that by setting $g_0^{\text{TPA}} = 0$ in Eqs. D4, D5 and D6, we recover exactly the same expressions for the ring resonator [48].

3. System at threshold

The onset of the oscillations of a pair of side modes $\mathcal{B}_{\pm\alpha'}$ can be determined by studying the linear stability around the trivial equilibrium, i.e., $\mathcal{B}_{\pm\alpha'}^s = 0$. This technique consists in adding a small time-dependent perturbation $\delta\mathcal{B}_{\pm\alpha'}(t)$ to the stationary equilibrium, and the set of parameters leading to the divergence of $\delta\mathcal{B}_{\pm\alpha'}(t)$ defines the threshold for side mode oscillations. Hence, the mode amplitude $\mathcal{B}_{\alpha'}(t)$ is written as

$$\mathcal{B}_{\alpha'}(t) = \mathcal{B}_{\alpha'}^s \delta_{\alpha',0} + \delta\mathcal{B}_{\alpha'}(t), \quad (\text{D10})$$

and replaced in Eq. D2, which gives

$$\begin{aligned} \frac{d\delta\mathcal{B}_{\alpha'}(t)}{dt} = & - \left[\frac{\gamma_{\alpha'}}{2} - i\sigma_{\alpha'} \right] \delta\mathcal{B}_{\alpha'}(t) \\ & + iG_0 \sum_{\mu'\eta'} [\mathcal{B}_{\mu'}^s \delta_{\mu',0} + \delta\mathcal{B}_{\mu'}(t)] [\mathcal{B}_{\eta'}^s \delta_{\eta',0} + \delta\mathcal{B}_{\eta'}(t)]^* [\mathcal{B}_{\alpha'+\eta'-\mu'}^s \delta_{\alpha'+\eta'-\mu',0} + \delta\mathcal{B}_{\alpha'+\eta'-\mu'}(t)] \\ & - \left[\frac{\gamma_{\alpha'}}{2} - i\sigma_{\alpha'} \right] \mathcal{B}_{\alpha'}^s \delta_{\alpha',0} + \frac{\gamma_{\alpha'}}{2} \mathcal{F}_{\alpha'} \delta_{\alpha',0}, \end{aligned} \quad (\text{D11})$$

where we have written explicitly the time derivative operator for the sake of clarity. By keeping only terms linear in $\delta\mathcal{B}$, and using the steady state solution of the central mode in Eq. D3, we get

$$\frac{d\delta\mathcal{B}_{\alpha'}(t)}{dt} = - \left[\frac{\gamma_{\alpha'}}{2} - i\sigma_{\alpha'} \right] \delta\mathcal{B}_{\alpha'}(t) + iG_0 \left[2|\mathcal{B}_0^s|^2 \delta\mathcal{B}_{\alpha'}(t) + \mathcal{B}_0^{s2} \delta\mathcal{B}_{-\alpha'}^*(t) \right] \quad (\text{D12})$$

For studying the dynamical behavior of the time-dependent perturbations, Eq. D12 can be rewritten in a more convenient form by making the transformations

$$\begin{aligned} \mathcal{C}_0^s &= \mathcal{B}_0^s \\ \delta\mathcal{C}_{\alpha'}(t) &= \delta\mathcal{B}_{\alpha'}(t) e^{i(\sigma_0 - \sigma_{\alpha'} + \frac{1}{2}\bar{\omega}_{\alpha'})t}, \end{aligned} \quad (\text{D13})$$

with

$$\bar{\omega}_{\alpha'} = 2\omega_0 - \omega_{\alpha'} - \omega_{-\alpha'}. \quad (\text{D14})$$

Moreover, in order to simplify the stability analysis, we replace the loss rates of the side modes $\gamma_{\pm\alpha'}$ by γ_0 , which is a good approximation when γ does not have strong fluctuations within the interval $[-\alpha', +\alpha']$. Equation D12 is finally turned into

$$\frac{d\delta\mathcal{C}_{\alpha'}(t)}{dt} = \left[i \left(\sigma_0 + \frac{1}{2}\bar{\omega}_{\alpha'} \right) - \frac{\gamma_0}{2} \right] \delta\mathcal{C}_{\alpha'}(t) + iG_0 \left[2|\mathcal{C}_0^s|^2 \delta\mathcal{C}_{\alpha'}(t) + \mathcal{C}_0^{s2} \delta\mathcal{C}_{-\alpha'}^*(t) \right]. \quad (\text{D15})$$

Notice that the coefficients of Eq. D15 are invariant to the change $\alpha' \rightarrow -\alpha'$ because $\bar{\omega}_{\alpha'} = \bar{\omega}_{-\alpha'}$, therefore, the dynamics of the side mode perturbations are described by the following two linearized equations

$$\begin{aligned} \frac{d\delta\mathcal{C}_{\alpha'}(t)}{dt} &= M_1 \delta\mathcal{C}_{\alpha'}(t) + M_2 \delta\mathcal{C}_{-\alpha'}^*(t) \\ \frac{d\delta\mathcal{C}_{-\alpha'}^*(t)}{dt} &= M_2^* \delta\mathcal{C}_{\alpha'}(t) + M_1^* \delta\mathcal{C}_{-\alpha'}^*(t), \end{aligned} \quad (\text{D16})$$

where

$$\begin{aligned} M_1 &= -\frac{\gamma_0}{2} + i\left(\sigma_0 + \frac{1}{2}\bar{\omega}_{\alpha'}\right) + 2iG_0|C_0^s|^2 \\ M_2 &= iG_0C_0^{s2}. \end{aligned} \quad (\text{D17})$$

The stability of the trivial equilibrium is then assessed by analyzing if the perturbation decays to zero, which means that such equilibrium is stable and there are no side mode oscillations, or if the perturbation diverges, meaning that the trivial equilibrium is unstable thus leading to the onset of side mode oscillations. This is carried out by writing

$$\begin{aligned} \delta C_{\alpha'}(t) &= e^{\lambda t} \delta C'_{\alpha'} \\ \delta C_{-\alpha'}^*(t) &= e^{\lambda t} \delta C'^*_{-\alpha'}, \end{aligned} \quad (\text{D18})$$

which together with Eq. D16 sets the following 2×2 eigenvalue problem

$$\begin{bmatrix} M_1 & M_2 \\ M_2^* & M_1^* \end{bmatrix} \begin{bmatrix} \delta C'_{\alpha'} \\ \delta C'^*_{-\alpha'} \end{bmatrix} = \lambda \begin{bmatrix} \delta C'_{\alpha'} \\ \delta C'^*_{-\alpha'} \end{bmatrix}. \quad (\text{D19})$$

The solutions for λ in Eq. D19 are readily found

$$\lambda_{\pm} = \text{Re}\{M_1\} \pm \sqrt{|M_2|^2 - \text{Im}\{M_1\}^2} = \frac{\gamma_0}{2} - 2g_0^{\text{TPA}2} |C_0^s|^2 \pm \sqrt{(g_0^{\text{TPA}2} - 3g_0^2) |C_0^s|^4 - 4g_0 |C_0^s|^2 \Delta_{\alpha'} - \Delta_{\alpha'}^2}, \quad (\text{D20})$$

where we have defined

$$\Delta_{\alpha'} = \sigma_0 + \frac{1}{2}\bar{\omega}_{\alpha'}. \quad (\text{D21})$$

The divergence of Eq. D18, i.e., the onset of the side mode oscillations, is clearly obtained when $\text{Re}\{\lambda_+\} > 0$, which in terms of the system parameters reads

$$\mathcal{S}_{\alpha'} = 12|G_0|^2 |C_0^s|^4 + 8(2\Delta_{\alpha'}g_0 + \gamma_0g_0^{\text{TPA}}) |C_0^s|^2 + 4\Delta_{\alpha'}^2 + \gamma_0^2 < 0. \quad (\text{D22})$$

The zeros of Eq. D22 determine the boundaries in which the trivial equilibrium becomes unstable. Therefore, by defining $\tilde{B} = |C_0^s|^2$, these boundaries are the solutions of the quadratic equation $\mathcal{S}_{\alpha'}(\tilde{B}) = 0$, i.e.,

$$\tilde{B}_{\pm} = \frac{-(2\Delta_{\alpha'}g_0 + \gamma_0g_0^{\text{TPA}}) \pm \frac{1}{2}\sqrt{4(2\Delta_{\alpha'}g_0 + \gamma_0g_0^{\text{TPA}})^2 - 3|G_0|^2(4\Delta_{\alpha'}^2 + \gamma_0^2)}}{3|G_0|^2}. \quad (\text{D23})$$

Notice that Eqs. D22 and D23 reduce exactly to the same corresponding expressions reported in Ref. [48] for $g_0^{\text{TPA}} = 0$. The minimum mode power leading to side mode oscillation is determined by the equation

$$\frac{\partial \tilde{B}_-}{\partial \Delta_{\alpha'}} = 0. \quad (\text{D24})$$

In terms of the fundamental CCW parameters and the actual momentum index (no shifted), this modal threshold power for comb generation is found to be

$$|\mathcal{A}_{\alpha_0}|_{\text{th}}^2 = \frac{\gamma_{\alpha_0}}{2g_{\alpha_0}} f(\kappa) = \frac{\epsilon V_c}{2ln_{g,\alpha_0}n_2Q_{\alpha_0}} f(\kappa), \quad (\text{D25})$$

where $Q_{\alpha_0} = \omega_{\alpha_0}/\gamma_{\alpha_0}$ is the quality factor of the driven CCW normal mode α_0 , and $f(\kappa)$ is a function of κ only

$$f(\kappa) = \frac{\sqrt{1 + \kappa^2} + 2\kappa}{1 - 3\kappa^2}, \quad (\text{D26})$$

From Eqs. D25 and D26 we clearly see that, as far as the threshold is concerned, TPA increases the minimum power required to start comb generation. The corresponding driven amplitude threshold $|\mathcal{F}_{\alpha_0}|_{\text{th}}^2(\sigma_{\alpha_0})$, which depends on the frequency detuning between the external laser and driven mode, is obtained by replacing Eq. D25 on Eq. D4 and recalling that $|\mathcal{A}| = |\mathcal{B}|$, thus

$$|\mathcal{F}_{\alpha_0}|_{\text{th}}^2(\sigma_{\alpha_0}) = \frac{2\sigma_{\alpha_0}^2}{g_{\alpha_0}\gamma_{\alpha_0}} f(\kappa) + \frac{2\sigma_{\alpha_0}}{g_{\alpha_0}} f^2(\kappa) + \frac{\gamma_{\alpha_0}}{2g_{\alpha_0}} f(\kappa) + \frac{g_{\alpha_0}^{\text{TPA}}\gamma_{\alpha_0}}{g_{\alpha_0}^2} f^2(\kappa) + \frac{|G_{\alpha_0}|^2\gamma_{\alpha_0}}{2g_{\alpha_0}^3} f^3(\kappa). \quad (\text{D27})$$

The optimal detuning that leads to the absolute minimal driven amplitude, required by comb generation, is easily found by solving the equation $\partial|\mathcal{F}_{\alpha_0}|_{\text{th}}^2/\partial\sigma_{\alpha_0} = 0$, and it is given by

$$\sigma_{\alpha_0}^{\text{th}} = -\frac{\gamma_{\alpha_0}}{2}f(\kappa), \quad (\text{D28})$$

Equation D28 shows that in presence of TPA, the optimal laser detuning to start frequency combs is red-shifted.

A closer look to Eq. D25 evidences that $|\mathcal{A}_{\alpha_0}|_{\text{th}}^2$ depends actually on the effective area of the cavity mode

$$|\mathcal{A}_{\alpha_0}|_{\text{th}}^2 = \frac{\epsilon A_{\text{eff}}}{2n_{g,\alpha_0}n_2Q_{\alpha_0}}f(\kappa), \quad (\text{D29})$$

where the mode area $A_{\text{eff}} = V_c/l$ is widely employed in waveguide physics. Moreover, if we consider the limit of no TPA, i.e., $f(\kappa = 0) = 1$, and the limit of no internal nanostructure (homogeneous slab for photonic crystals) where the group index is very close to the actual refractive index of the dielectric n , i.e., $\epsilon = n^2 \simeq n_{g,\alpha_0}^2$, Eq. D29 becomes

$$|\mathcal{A}_{\alpha_0}|_{\text{th}}^2 = \frac{nA_{\text{eff}}}{2n_2Q_{\alpha_0}}, \quad (\text{D30})$$

which is exactly the same threshold expression (in Watts) for the internal mode power in a non-linear ring resonator [46].

4. Role of dispersion in frequency comb generation

In order to the boundaries of Eq. D23 be real and positive, the discriminant of the square root has to be positive and the term $(2\Delta_{\alpha'}g_0 + \gamma_0g_0^{\text{TPA}})$ has to be negative. Both conditions are satisfied if

$$\Delta_{\alpha'} < \sigma_{\text{cr}}\rho(\kappa), \quad (\text{D31})$$

where the critical detuning σ_{cr} is defined as

$$\sigma_{\text{cr}} = -\frac{\gamma_0\sqrt{3}}{2}, \quad (\text{D32})$$

If the dispersion relation $\omega_{\alpha'}$ is expanded in Taylor series around ω_0 up to third order, we have

$$\omega_{\alpha'} = \omega_0 + \zeta_1\alpha' + \frac{\zeta_2}{2}\alpha'^2 + \frac{\zeta_3}{3!}\alpha'^3, \quad (\text{D33})$$

with ζ_1 , ζ_2 and ζ_3 representing the group velocity, group velocity dispersion and third order dispersion, respectively. Replacing Eq. D33 in Eq. D14 gives

$$\bar{\omega}_{\alpha'} = -\zeta_2\alpha'^2, \quad (\text{D34})$$

turning the condition of Eq. D31 into

$$-\zeta_2\alpha'^2 < 2[\sigma_{\text{cr}}\rho(\kappa) - \sigma_0]. \quad (\text{D35})$$

For normal dispersion $\zeta_2 < 0$ and Eq. D35 defines the following condition for α'

$$\alpha' < \sqrt{\frac{2}{|\zeta_2|}[\sigma_{\text{cr}}\rho(\kappa) - \sigma_0]} = \alpha'_{\text{max}}, \quad (\text{D36})$$

while for anomalous dispersion $\zeta_2 > 0$ the condition determined by Eq. D35 reads

$$\alpha' > \sqrt{\frac{2}{|\zeta_2|}[\sigma_0 - \sigma_{\text{cr}}\rho(\kappa)]} = \alpha'_{\text{min}}. \quad (\text{D37})$$

Therefore, from Eqs. D36 and D37, we clearly see that if the system is pumped where dispersion is normal, there is an upper bound on the side mode momentum, thus constraining the spanning of the frequency comb. Nevertheless, if the dispersion is anomalous, there is no upper bound on the momentum for side mode oscillations, and the comb generation regime is easily achieved.

Appendix E: Lugiato-Lefever equation

The corresponding spatio-temporal equation for the non-linear formalism presented in Sec. C can be obtained by following the derivation of Ref. [49]. We start from the system of coupled mode equations in Eq. C39, which can be rewritten as

$$\dot{\mathcal{B}}_\alpha(t) + \left[\frac{\gamma_\alpha}{2} - i\sigma_\alpha \right] \mathcal{B}_\alpha(t) - ig_{\alpha_0}(1 + i\kappa) \sum_{\mu\eta\xi} \mathcal{B}_\mu(t)\mathcal{B}_\eta^*(t)\mathcal{B}_\xi(t)\delta_{\xi,\alpha+\eta-\mu} - \frac{\gamma_\alpha}{2}\mathcal{F}_\alpha\delta_{\alpha,\alpha_0} = 0, \quad (\text{E1})$$

where we have explicitly considered the delta factor in the non-linear term and used Eqs. C36, C37, C38 and D9 to write $G_{\alpha_0} = g_{\alpha_0}(1 + i\kappa)$. We define the following spatio-temporal slowly-varying envelope along the waveguide direction

$$\psi(y, t) = \sum_\alpha \mathcal{B}_\alpha(t)e^{-i(\alpha-\alpha_0)y}, \quad (\text{E2})$$

from which we have

$$\frac{\partial\psi(y, t)}{\partial t} = \sum_\alpha \dot{\mathcal{B}}_\alpha(t)e^{-i(\alpha-\alpha_0)y}, \quad (\text{E3})$$

$$i^m \frac{\partial^m \psi(y, t)}{\partial y^m} = \sum_\alpha (\alpha - \alpha_0)^m \mathcal{B}_\alpha(t)e^{-i(\alpha-\alpha_0)y}. \quad (\text{E4})$$

Equation E1 is now replaced in Eq. E3 leading to

$$\frac{\partial\psi(y, t)}{\partial t} = \sum_\alpha \left[i\sigma_\alpha - \frac{\gamma_\alpha}{2} \right] \mathcal{B}_\alpha(t)e^{-i(\alpha-\alpha_0)y} + ig_{\alpha_0}(1 + i\kappa) \sum_{\mu\eta\xi} \mathcal{B}_\mu(t)e^{-i(\mu-\alpha_0)y}\mathcal{B}_\eta^*(t)e^{i(\eta-\alpha_0)y}\mathcal{B}_\xi(t)e^{-i(\xi-\alpha_0)y} + \frac{\gamma_{\alpha_0}}{2}\mathcal{F}_{\alpha_0}, \quad (\text{E5})$$

and because

$$|\psi(y, t)|^2\psi(y, t) = \sum_{\mu\eta\xi} \mathcal{B}_\mu(t)e^{-i(\mu-\alpha_0)y}\mathcal{B}_\eta^*(t)e^{i(\eta-\alpha_0)y}\mathcal{B}_\xi(t)e^{-i(\xi-\alpha_0)y}, \quad (\text{E6})$$

we readily get from Eq. E5

$$\frac{\partial\psi}{\partial t} = \sum_\alpha \left[i\sigma_\alpha - \frac{\gamma_\alpha}{2} \right] \mathcal{B}_\alpha(t)e^{-i(\alpha-\alpha_0)y} + ig_{\alpha_0}(1 + i\kappa)|\psi|^2\psi + \frac{\gamma_{\alpha_0}}{2}\mathcal{F}_{\alpha_0}, \quad (\text{E7})$$

where we have simplified the notation $\psi(y, t) \rightarrow \psi$. By writing the mode detuning as

$$\sigma_\alpha = \Omega_0 - \omega_\alpha = \Omega_0 - \omega_{\alpha_0} - (\omega_\alpha - \omega_{\alpha_0}) = \sigma_{\alpha_0} - (\omega_\alpha - \omega_{\alpha_0}), \quad (\text{E8})$$

and expanding the last term in Taylor series around ω_{α_0}

$$\omega_\alpha - \omega_{\alpha_0} = \sum_m \frac{\zeta_m}{m!} (\alpha - \alpha_0)^m, \quad (\text{E9})$$

Eq. E7 is turned into

$$\begin{aligned} \frac{\partial\psi}{\partial t} &= ig_{\alpha_0}(1 + i\kappa)|\psi|^2\psi + i\sigma_{\alpha_0} \sum_\alpha \mathcal{B}_\alpha(t)e^{-i(\alpha-\alpha_0)y} - \sum_\alpha \frac{\gamma_\alpha}{2}\mathcal{B}_\alpha(t)e^{-i(\alpha-\alpha_0)y} \\ &\quad - i \sum_m \frac{\zeta_m}{m!} \sum_\alpha (\alpha - \alpha_0)^m \mathcal{B}_\alpha(t)e^{-i(\alpha-\alpha_0)y} + \frac{\gamma_{\alpha_0}}{2}\mathcal{F}_{\alpha_0}. \end{aligned} \quad (\text{E10})$$

If we use Eqs. E2 and E4, and assume an overall losses given by the loss rate at the pump frequency, i.e., $\gamma_\alpha = \gamma_{\alpha_0}$ [61], Eq. E10 takes the following form

$$\frac{\partial\psi}{\partial t} = \left(i\sigma_{\alpha_0} - \frac{\gamma_{\alpha_0}}{2} \right) \psi + ig_{\alpha_0}(1 + i\kappa)|\psi|^2\psi + \zeta_1 \frac{\partial\psi}{\partial y} + i\frac{\zeta_2}{2} \frac{\partial^2\psi}{\partial y^2} + \sum_{m=3} i^{m-1} \frac{\zeta_m}{m!} \frac{\partial^m\psi}{\partial y^m} + \frac{\gamma_{\alpha_0}}{2}\mathcal{F}_{\alpha_0}, \quad (\text{E11})$$

where the group velocity ζ_1 and the group velocity dispersion ζ_2 have been written explicitly. In order to get rid of the first spatial-derivative term we change to a moving reference frame with velocity ζ_1 , i.e.,

$$\begin{aligned} y' &= y + \zeta_1 t \\ t' &= t \end{aligned} \quad (\text{E12})$$

which gives

$$\begin{aligned} \frac{\partial}{\partial t} &= \frac{\partial}{\partial t'} + \zeta_1 \frac{\partial}{\partial y'}, \\ \frac{\partial}{\partial y} &= \frac{\partial}{\partial y'}. \end{aligned} \quad (\text{E13})$$

Replacing Eq. E13 in Eq. E11, and introducing the normalized detuning $\varsigma = -2\sigma_{\alpha_0}/\gamma_{\alpha_0}$, we arrive to

$$\frac{\partial \psi}{\partial t'} = -(1 + i\varsigma) \frac{\gamma_{\alpha_0}}{2} \psi + ig_{\alpha_0}(1 + i\kappa)|\psi|^2\psi + i \frac{\zeta_2}{2} \frac{\partial^2 \psi}{\partial y'^2} + \sum_{m=3} i^{m-1} \frac{\zeta_m}{m!} \frac{\partial^m \psi}{\partial y'^m} + \frac{\gamma_{\alpha_0}}{2} \mathcal{F}_{\alpha_0}. \quad (\text{E14})$$

By defining the quantities $\Psi = \sqrt{2g_{\alpha_0}/\gamma_{\alpha_0}}\psi$, $F = \sqrt{2g_{\alpha_0}/\gamma_{\alpha_0}}\mathcal{F}_{\alpha_0}$, $\varrho_m = -2\zeta_m/\gamma_{\alpha_0}$ and $\tau = (\gamma_{\alpha_0}/2)t'$ we finally get the normalized Lugiato-Lefever equation with non-linear losses (TPA) and high-order dispersion

$$\frac{\partial \Psi}{\partial \tau} = -(1 + i\varsigma)\Psi + i(1 + i\kappa)|\Psi|^2\Psi - i \frac{\varrho_2}{2} \frac{\partial^2 \Psi}{\partial y'^2} + \sum_{m=3} i^{m+1} \frac{\varrho_m}{m!} \frac{\partial^m \Psi}{\partial y'^m} + F \quad (\text{E15})$$

Appendix F: Soliton dynamics

We report in Figs. 5 and 6 the spectral dynamics of soliton formation for the two relevant cases III and IV, respectively, presented in Figs. 2 and 3 in the manuscript. Panels correspond to different times (in ns units) during the transient dynamics and the associated envelope function along the waveguide direction is shown in the inset.

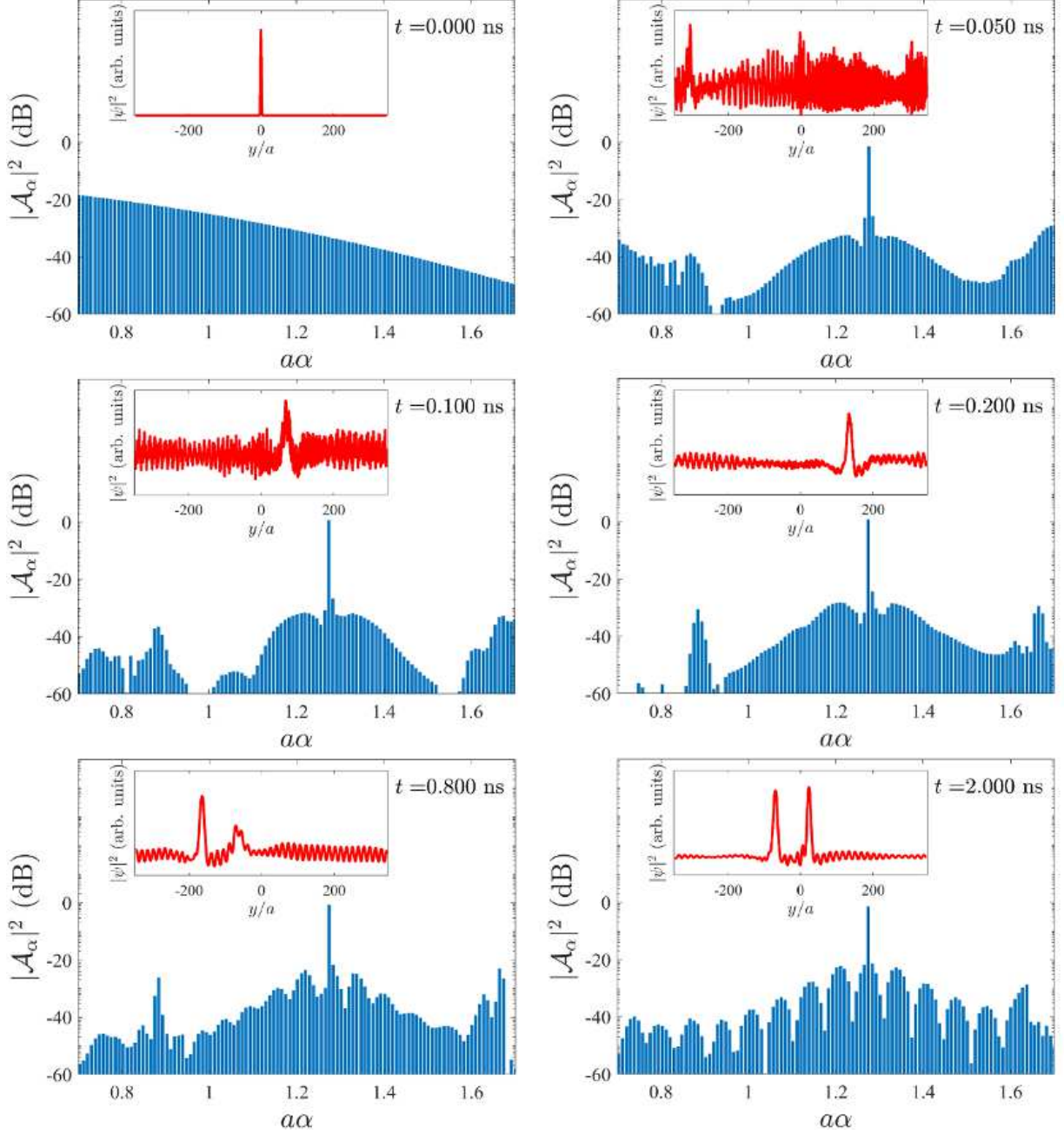


FIG. 5. Transient dynamics of the spectral components for the molecule soliton of two pulses. The corresponding envelope function is shown in the inset. $|A_\alpha|^2$ is given in threshold units and the initial condition ($t = 0$) is the sharp Gaussian pulse $\psi(y, t = 0) = \exp[-0.5(y/\sqrt{3}a)^2]$.

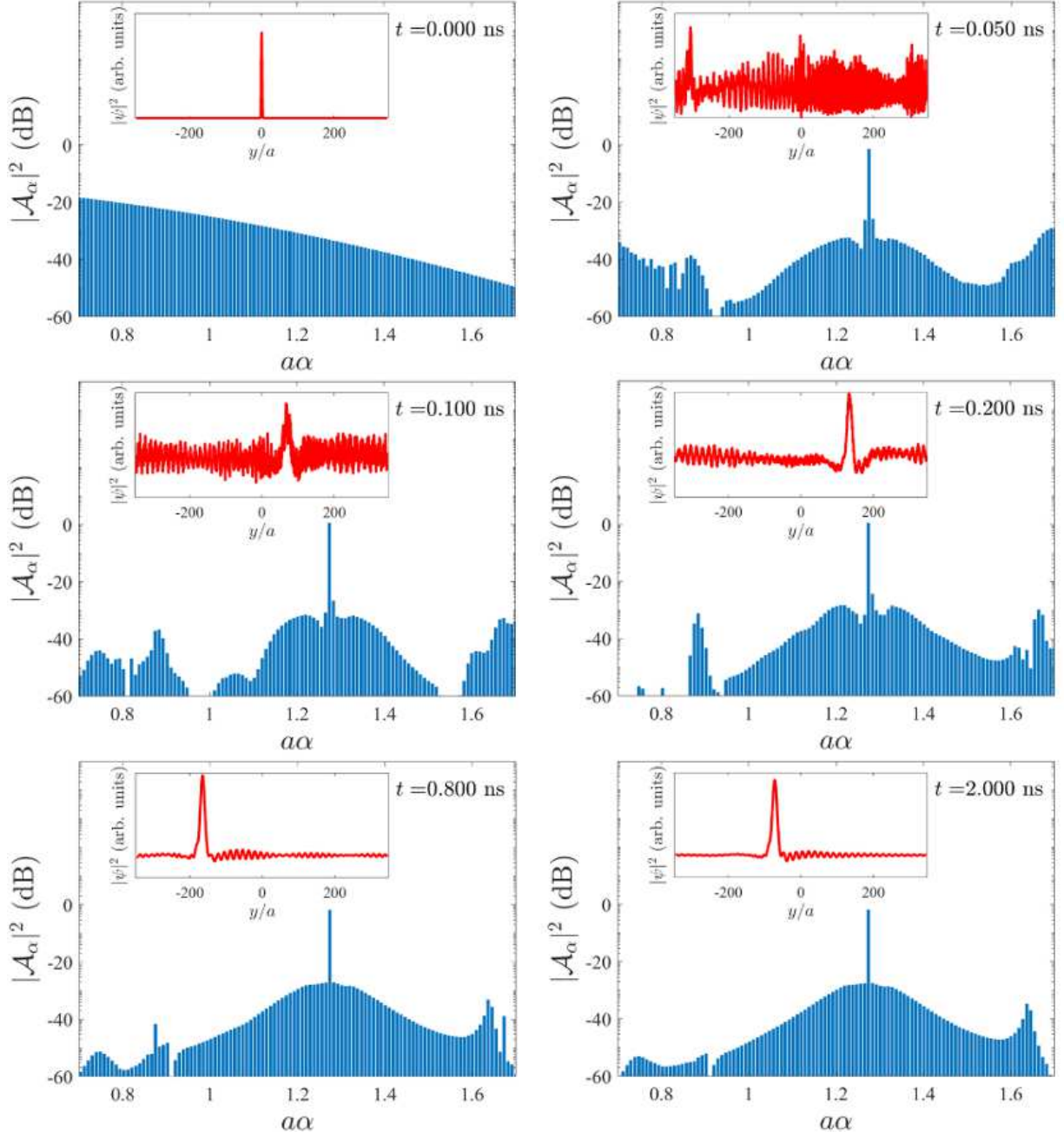


FIG. 6. Transient dynamics of the spectral components for a single soliton pulse. The corresponding envelope function is shown in the inset. $|A_\alpha|^2$ is given in threshold units and the initial condition ($t = 0$) is the sharp Gaussian pulse $\psi(y, t = 0) = \exp[-0.5(y/\sqrt{3}a)^2]$.

[1] P. Del’Haye, A. Schliesser, O. Arcizet, T. Wilken, R. Holzwarth, and T. J. Kippenberg, “Optical frequency comb generation from a monolithic microresonator,” *Nature* **450**, 1214 (2007).

[2] Ian Coddington, Nathan Newbury, and William Swann, “Dual-comb spectroscopy,” *Optica* **3**, 414 (2016).

[3] Nathalie Picqué and Theodor W. Hänsch, “Frequency comb spectroscopy,” *Nat. Photonics* **13**, 146 (2019).

- [4] Pablo Marin-Palomo, Juned N. Kemal, Maxim Karpov, Arne Kordts, Joerg Pfeifle, Martin H. P. Pfeiffer, Philipp Trocha, Stefan Wolf, Victor Brasch, Miles H. Anderson, Ralf Rosenberger, Kovendhan Vijayan, Wolfgang Freude, Tobias J. Kippenberg, and Christian Koos, “Microresonator-based solitons for massively parallel coherent optical communications,” *Nature* **546**, 274 (2017).
- [5] P. Trocha, M. Karpov, D. Ganin, M. H. P. Pfeiffer, A. Kordts, S. Wolf, J. Krockenberger, P. Marin-Palomo, C. Weimann, S. Randel, W. Freude, T. J. Kippenberg, and C. Koos, “Ultrafast optical ranging using microresonator soliton frequency combs,” *Science* **359**, 887 (2018).
- [6] Daryl T. Spencer, Tara Drake, Travis C. Briles, Jordan Stone, Laura C. Sinclair, Connor Fredrick, Qing Li, Daron Westly, B. Robert Ilic, Aaron Bluestone, Nicolas Volet, Tin Komljenovic, Lin Chang, Seung Hoon Lee, Dong Yoon Oh, Myoung-Gyun Suh, Ki Youl Yang, Martin H. P. Pfeiffer, Tobias J. Kippenberg, Erik Norberg, Luke Theogarajan, Kerry Vahala, Nathan R. Newbury, Kartik Srinivasan, John E. Bowers, Scott A. Diddams, and Scott B. Papp, “An optical-frequency synthesizer using integrated photonics,” *Nature* **557**, 81 (2018).
- [7] Andrew J. Benedick, Guoqing Chang, Jonathan R. Birge, Li-Jin Chen, Alexander G. Glenday, Chih-Hao Li, David F. Phillips, Andrew Szentgyorgyi, Sylvain Korzenik, Gabor Furesz, Ronald L. Walsworth, and Franz X. Kärtner, “Visible wavelength astro-comb,” *Opt. Express* **18**, 19175 (2010).
- [8] Ewelina Obrzud, Monica Rainer, Avet Harutyunyan, Miles H. Anderson, Junqiu Liu, Michael Geiselmann, Bruno Chazelas, Stefan Kundermann, Steve Lecomte, Massimo Cecconi, Adriano Ghedina, Emilio Molinari, Francesco Pepe, François Wildi, François Bouchy, Tobias J. Kippenberg, and Tobias Herr, “A microphotonic astrocomb,” *Nat. Photonics* **13**, 31 (2019).
- [9] Ewelina Obrzud, Steve Lecomte, and Tobias Herr, “Temporal solitons in microresonators driven by optical pulses,” *Nat. Photonics* **11**, 600 (2017).
- [10] T. J. Kippenberg, R. Holzwarth, and S. A. Diddams, “Microresonator-based optical frequency combs,” *Science* **29**, 555 (2011).
- [11] Tobias J. Kippenberg, Alexander L. Gaeta, Michal Lipson, and Michael L. Gorodetsky, “Dissipative kerr solitons in optical microresonators,” *Science* **361**, 567 (2018).
- [12] A. G. Vladimirov, S. V. Gurevich, and M. Tlidi, “Effect of cherenkov radiation on localized-state interaction,” *Phys. Rev. A* **97**, 013816 (2018).
- [13] Pedro Parra-Rivas, Damia Gomila, Pere Colet, and Lendert Gelens, “Interaction of solitons and the formation of bound states in the generalized lugiato-lefever equation,” *Eur. Phys. J. D* **71**, 198 (2017).
- [14] Carles Milián, Yaroslav V. Kartashov, Dmitry V. Skryabin, and Lluís Torner, “Clusters of cavity solitons bounded by conical radiation,” *Phys. Rev. Lett.* **121**, 103903 (2018).
- [15] Mengjie Yu, Jae K. Jang, Yoshitomo Okawachi, Austin G. Griffith, Kevin Luke, Steven A. Miller, Xingchen Ji, Michal Lipson, and Alexander L. Gaeta, “Breather soliton dynamics in microresonators,” *Nat Commun.* **8**, 14569 (2017).
- [16] E. Lucas, M. Karpov, H. Guo, M. L. Gorodetsky, and T. J. Kippenberg, “Breathing dissipative solitons in optical microresonators,” *Nat Commun.* **8**, 736 (2017).
- [17] Hairun Guo, Erwan Lucas, Martin H. P. Pfeiffer, Maxim Karpov, Miles Anderson, Junqiu Liu, Michael Geiselmann, John D. Jost, and Tobias J. Kippenberg, “Intermode breather solitons in optical microresonators,” *Phys. Rev. X* **7**, 041055 (2017).
- [18] Daniel C. Cole, Erin S. Lamb, Pascal Del’Haye, Scott A. Diddams, and Scott B. Papp, “Soliton crystals in kerr resonators,” *Nat. Photonics* **11**, 671 (2017).
- [19] Maxim Karpov, Martin H. P. Pfeiffer, Hairun Guo, Wenle Weng, Junqiu Liu, and Tobias J. Kippenberg, “Dynamics of soliton crystals in optical microresonators,” *Nat. Phys.* **15**, pages1071 (2019).
- [20] T. Herr, V. Brasch, J. D. Jost, C. Y. Wang, N. M. Kondratiev, M. L. Gorodetsky, and T. J. Kippenberg, “Temporal solitons in optical microresonators,” *Nat. Photonics* **8**, 145 (2014).
- [21] Alexander L. Gaeta, Michal Lipson, and Tobias J. Kippenberg, “Photonic-chip-based frequency combs,” *Nat. Photonics* **13**, 158 (2019).
- [22] Stéphane Coen, Hamish G. Randle, Thibaut Sylvestre, and Miro Erkintalo, “Modeling of octave-spanning kerr frequency combs using a generalized mean-field lugiato-lefever model,” *Opt. Lett.* **38**, 37 (2013).
- [23] C. Milián and D.V. Skryabin, “Soliton families and resonant radiation in a micro-ring resonator near zero group-velocity dispersion,” *Opt. Express* **22**, 3732 (2014).
- [24] Pedro Parra-Rivas, Damià Gomila, François Leo, Stéphane Coen, and Lendert Gelens, “Third-order chromatic dispersion stabilizes kerr frequency combs,” *Opt. Lett.* **39**, 2971 (2014).
- [25] V. Brasch, M. Geiselmann, T. Herr, G. Lihachev, M. H. P. Pfeiffer, M. L. Gorodetsky, and T. J. Kippenberg, “Photonic chip-based optical frequency comb using soliton cherenkov radiation,” *Science* **351**, 357 (2016).
- [26] Mark A. Foster, Amy C. Turner, Jay E. Sharping, Bradley S. Schmidt, Michal Lipson, and Alexander L. Gaeta, “Broad-band optical parametric gain on a silicon photonic chip,” *Nature* **441**, 960 (2006).
- [27] Lin Zhang, Chengying Bao, Vivek Singh, Jianwei Mu, Changxi Yang, Anuradha M. Agarwal, Lionel C. Kimmerling, and Jurgen Michel, “Generation of two-cycle pulses and octave-spanning frequency combs in a dispersion-flattened micro-resonator,” *Opt. Lett.* **38**, 5122 (2013).
- [28] Yoshitomo Okawachi, Michael R. E. Lamont, Kevin Luke, Daniel O. Carvalho, Mengjie Yu, Michal Lipson, and Alexander L. Gaeta, “Bandwidth shaping of microresonator-based frequency combs via dispersion engineering,” *Opt. Lett.* **39**, 3535 (2014).
- [29] Ivan S. Grudin and Nan Yu, “Dispersion engineering of crystalline resonators via microstructuring,” *Optica* **2**, 221 (2015).
- [30] Daniel C. Cole, Alessandra Gatti, Scott B. Papp, Franco Prati, and Luigi Lugiato, “Theory of kerr frequency combs in fabry-perot resonators,” *Phys. Rev. A* **98**, 013831 (2018).
- [31] Su-Peng Yu, Hojoong Jung, Travis C. Briles, Srinivasan Kartik, and Scott B. Papp, “Photonic-crystal-reflector nano-resonators for kerr-frequency combs,” arXiv:1904.07289 (2019).
- [32] Amnon Yariv, Yong Xu, Reginald K. Lee, and Axel Scherer, “Coupled-resonator optical waveguide: a proposal and analysis,” *Opt. Lett.* **24**, 711 (1999).
- [33] Marin Soljačić, Steven G. Johnson, Shanhui Fan, Mihai Ibanescu, Erich Ippen, and J. D. Joannopoulos,

- “Photonic-crystal slow-light enhancement of nonlinear phase sensitivity,” *J. Opt. Soc. Am. B* **19**, 2052 (2002).
- [34] Yan Chen and Steve Blair, “Nonlinearity enhancement in finite coupled-resonator slow-light waveguides,” *Opt. Express* **12**, 3353 (2004).
- [35] D. O’Brien, M.D. Settle, T. Karle, A. Michaeli, M. Salib, and T.F. Krauss, “Coupled photonic crystal heterostructure nanocavities,” *Opt. Express* **15**, 1228 (2007).
- [36] Masaya Notomi, Eiichi Kuramochi, and Takasumi Tanabe, “Large-scale arrays of ultrahigh-q coupled nanocavities,” *Nat. Photonics* **2**, 741 (2008).
- [37] Nobuyuki Matsuda, Takumi Kato, Ken-ichi Harada, Hiroki Takesue, Eiichi Kuramochi, Hideaki Taniyama, and Masaya Notomi, “Slow light enhanced optical nonlinearity in a silicon photonic crystal coupled-resonator optical waveguide,” *Opt. Express* **19**, 19861 (2011).
- [38] Momchil Minkov and Vincenzo Savona, “Wide-band slow light in compact photonic crystal coupled-cavity waveguides,” *Optica* **2**, 631 (2015).
- [39] Yiming Lai, Mohamed Sabry Mohamed, Boshen Gao, Momchil Minkov, Robert W. Boyd, Vincenzo Savona, Romuald Houdré, and Antonio Badolato, “Ultra-wide-band structural slow light,” *Sci. Rep.* **8**, 14811 (2018).
- [40] Mohamed Sabry Mohamed, Yiming Lai, Momchil Minkov, Vincenzo Savona, Antonio Badolato, and Romuald Houdré, “Influence of disorder and finite-size effects on slow light transport in extended photonic crystal coupled-cavity waveguides,” *ACS Photonics* **5**, 4846 (2018).
- [41] Lucio Claudio Andreani and Dario Gerace, “Photonic-crystal slabs with a triangular lattice of triangular holes investigated using a guided-mode expansion method,” *Phys. Rev. B* **73**, 235114 (2006).
- [42] Lumerical Solutions, Inc. (2019).
- [43] Weiwei Song, Ryan A. Integlia, and Wei Jiang, “Slow light loss due to roughness in photonic crystal waveguides: An analytic approach,” *Phys. Rev. B* **82**, 235306 (2010).
- [44] Nick K. Hon, Richard Soref, and Bahram Jalali, “The third-order nonlinear optical coefficients of si, ge, and si_{1-x}ge_x in the midwave and longwave infrared,” *J. Appl. Phys.* **110**, 011301 (2011).
- [45] Yao Zhang and Baojun Li, “Photonic crystal-based bending waveguides for optical interconnections,” *Opt. Express* **14**, 5723 (2006).
- [46] Yanne K. Chembo, “Quantum dynamics of kerr optical frequency combs below and above threshold: Spontaneous four-wave mixing, entanglement, and squeezed states of light,” *Phys. Rev. A* **93**, 033820 (2016).
- [47] Yanne K. Chembo, Dmitry V. Strekalov, and Nan Yu, “Spectrum and dynamics of optical frequency combs generated with monolithic whispering gallery mode resonators,” *Phys. Rev. Lett.* **104**, 103902 (2010).
- [48] Yanne K. Chembo and Nan Yu, “Modal expansion approach to optical-frequency-comb generation with monolithic whispering-gallery-mode resonators,” *Phys. Rev. A* **82**, 033801 (2010).
- [49] Yanne K. Chembo and Curtis R. Menyuk, “Spatiotemporal lugiato-lefever formalism for kerr-comb generation in whispering-gallery-mode resonators,” *Phys. Rev. A* **87**, 053852 (2013).
- [50] Ryan K. W. Lau, Michael R. E. Lamont, Yoshitomo Okawachi, and Alexander L. Gaeta, “Effects of multiphoton absorption on parametric comb generation in silicon microresonators,” *Opt. Lett.* **40**, 2778 (2015).
- [51] Ambareesh Sahoo, Samudra Roy, and Govind P. Agrawal, “Perturbed dissipative solitons: A variational approach,” *Phys. Rev. A* **96**, 013838 (2017).
- [52] T. Herr, K. Hartinger, J. Riemensberger, C. Y. Wang, E. Gavartin, R. Holzwarth, M. L. Gorodetsky, and T. J. Kippenberg, “Universal formation dynamics and noise of kerr-frequency combs in microresonators,” *Nat. Photonics* **6**, 480 (2012).
- [53] T. Hansson, D. Modotto, and S. Wabnitz, “On the numerical simulation of kerr frequency combs using coupled mode equations,” *Opt. Commun.* **312**, 134 (2014).
- [54] Cyril Godey, Irina V. Balakireva, Aurélien Coillet, and Yanne K. Chembo, “Stability analysis of the spatiotemporal lugiato-lefever model for kerr optical frequency combs in the anomalous and normal dispersion regimes,” *Phys. Rev. A* **89**, 063814 (2014).
- [55] Myoung-Gyun Suh and Kerry Vahala, “Gigahertz-repetition-rate soliton microcombs,” *Optica* **5**, 65 (2018).
- [56] Philip Trøst Kristensen and Stephen Hughes, “Modes and mode volumes of leaky optical cavities and plasmonic nanoresonators,” *ACS Photon.* **1**, 2 (2014).
- [57] John D. Joannopoulos, Steven G. Johnson, Joshua N. Winn, and Robert D. Meade, *Photonic Crystals: Molding the Flow of Light*, 2nd ed. (Princeton University Press, 2008) Chap. 2-3.
- [58] Robert W. Boyd, *Nonlinear optics*, 3rd ed. (Academic Press, 2007).
- [59] Rigorously, one should employ the set of Wannier functions to carry out the expansion of Eq. C18, as the cavity modes do not define a complete orthogonal set of functions. Nevertheless, for strongly localized cavity modes this expansion describes very well the physics of a CCW system.
- [60] Pierre Colman, “Field renormalization in photonic crystal waveguides,” *Phys. Rev. A* **92**, 013827 (2015).
- [61] We are ultimately assuming that the loss rates do not depend on the frequency or, equivalently, on the momentum. Such losses may be given by γ_{α_0} or by any reliable constant value within the Brillouin zone of the CCW.